

**UNIVERSITY OF TURKISH AERONAUTICAL ASSOCIATION
INSTITUTE OF SCIENCE AND TECHNOLOGY**

**EXPERIMENTAL AND CFD ANALYSIS OF NANO-FLUID INSIDE INCLINED
ENCLOSURE**

Master Thesis

Safaa Rashid SALIH

Institute of Science and Technology

Mechanical and Aeronautical Engineering Department

JULY, 2017

**UNIVERSITY OF TURKISH AERONAUTICAL ASSOCIATION
INSTITUTE OF SCIENCE AND TECHNOLOGY**

**EXPERIMENTAL AND CFD ANALYSIS OF NANO-FLUID INSIDE INCLINED
ENCLOSUER**

Master Thesis

Safaa Rashid SALIH

1403730055


**IN PARTIAL FULFILLMENT OF THE REQUIREMENT FOR THE
DEGREE OF MASTER OF SCIENCE IN MECHANICAL AND
AERONAUTICAL ENGINEERING**

Thesis Supervisor: Assist. Prof. Dr. Sudantha BALAGE

Thesis Co. Supervisor: Assist. Prof. Dr. Amar HAMEED

Türk Hava Kurumu Üniversitesi Fen Bilimleri Enstitüsü'nün 1403730055 numaralı Yüksek Lisans öğrencisi, "Safaa Rashid Salih" ilgili yönetmeliklerin belirlediği gerekli tüm şartları yerine getirdikten sonra hazırladığı "Experimental and CFD Analysis of Nano-fluid inside Inclined Enclosure" başlıklı tezini, aşağıda imzaları bulunan jüri önünde başarı ile sunmuştur.

Tez Danışmanı : Yrd. Doç. Dr. Sudantha BALAGE
Türk Hava Kurumu Üniversitesi



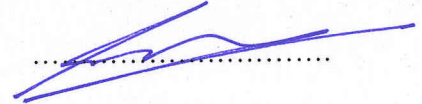
Eş Danışmanı : Yrd. Doç. Dr. Amar HAMEED
KTO Karatay Üniversitesi



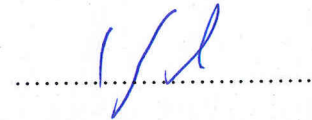
Jüri Üyeleri : Yrd. Doç. Dr. Ece Aylı İNCE
Türk Hava Kurumu Üniversitesi



Yrd. Doç. Dr. Sudantha BALAGE
Türk Hava Kurumu Üniversitesi



Yrd. Doç. Dr. Munir ELFARRA
Ankara Yıldırım Beyazıt Üniversitesi



Tez Savunma Tarihi: 20.07.2017

STATEMENT OF NON-PLAGIARISM PAGE

I hereby declare that all information in this document as my Master's Thesis, called **"EXPERIMENTAL AND CFD ANALYSIS OF NANO-FLUID INSIDE INCLINED ENCLOSUER."** has been obtained and presented in accordance with academic rules and ethical conduct. I have fully cited and referenced all the material and results that are not original to this work.



Date 20/07/2017

Safaa Rashid Salih.

ACKNOWLEDGEMENTS

I am grateful to The Almighty GOD for helping me to complete this thesis. My Lord mercy and peace be upon our leader Mohammed peace is upon on him, who invites us to science and wisdom, and members of his family and his followers.

I would like to thank my parents for supporting me throughout my academic career. Without their moral support interest, and encouragement for my academic work, the completion of this effort would not have been possible.

My ambition to obtain a master degree was fulfilled mainly because of the support and guidance I received from my former advisors, Assist. Prof. Dr. Sudantha Balage and Prof. Dr.Amar Hasan-Hameed. They have helped me at various stages during my studies and this includes providing me with a well-defined thesis problem, equipping me with the necessary tools and techniques for achieving my objectives, and willingly sharing his knowledge and ideas with me. Their active participation at every facet of my research work and mentoring has shaped my overall research outlook. I am extremely grateful to them for being my advisers during their stay at University of Turkish Aeronautical Association.

Thanks to my wife, for being everything in my life, for his patience, supporting and invaluable assistance.

I would like to express my profound gratitude to my kids AYA, Rahaaf and Aws whom this work is dedicated, for every time they needed me, but I wasn't there for missing me throughout my study.

I would also like to thank Eng. Jamal H-Salih Director of (Salahaddin Power Transmission Network), Eng. Mustafa J Ibraheem assists Director of (Salahaddin Power Transmission Network) and my friend Eng Othman K-Hassan for helping me. I would also like to thank my friend Eng Mohammed Y-Nawaaf for his unlimited support through and supplying a huge amount of information that needs to this work.

July 2017

Safaa Rashid SALIH

Table of Contents

ACKNOWLEDGEMENTS	IV
List of Figures	VIII
LIST OF TABLES	X
LIST OF SYMBOLS	XI
ABSTRACT	XIII
ÖZET	XV
CHAPTER ONE	1
1. INTRODUCTION	1
1.1 Introduction	1
1.2 Problem Statement	3
1.3 Thesis Objective.....	4
1.4 Organization of the Thesis	5
CHAPTER TWO	6
LITERATURE REVIEW	6
2.1Introduction	6
2.2 Literature review of solar collectors based nano-fluid in the recent years.	7
2.3 Conclusion of literature review.....	18
CHAPTER THREE.....	19
Simulation And Experimental of System.....	19
3.1 Introduction.....	19
3.2 Design of models	20
3.3 Grid Generation.....	21
3.4 FLUENT modeling methodology	24
3.4.1 Inclined Angle.....	24
3.4.2. Properties of materials used in simulation.....	25

3.4.2.1 Calculation of nano-fluid properties.	25
3.4.2.1.1 Thermal Conductivity of nano-fluid in $W \cdot (m \cdot K)^{-1}$	25
3.4.2.1.2 Dynamic viscosity of nano-fluid in $(Pa \cdot s)$	25
3.4.2.1.3 Specific heat and density of nano-fluid in $J \cdot (kg \cdot K)^{-1}$ and $(kg \cdot m^{-3})$	26
3.4.2.1.4 Coefficient of volume expansion of the nano-fluid in $(1/k)$	26
3.4.2.1.5 Absorption and scattering coefficients of the nano-fluid in $(1/m)$	27
3.4.2.2 Properties of liquid water.	28
3.4.2.3 Properties of copper tube.	28
3.4.2.4 Properties of glass tube.	28
3.4.3 Boussinesq approximation.	29
3.4.4 Modeling Natural Convection in enclosure Domain.	29
3.4.5 Energy and momentum Equation in ANSYS FLUENT software.	30
3.4.6 Radiative Transfer Equation.	30
3.4.7 The Boundary Condition with Semi Transparent Wall.	31
3.4.8 Heat loss analysis.	32
3.4.9 The overall heat transfer loss coefficient (UL)UDF.	34
3.5 EXPERIMENTAL INVESTIGATION.	35
3.5.1 Introduction.	35
3.5.2 General specifications of the experimental device.	35
3.5.3 Glass tube.	36
3.5.4 Copper tube.	36
3.5.5 Nano-Fluid.	36
3.5.6 Device Holder.	36
3.5.7 The measurement system.	37
3.5.7.1 Water Flow Meter.	37

3.5.7.2	Temperature measuring system (Thermocouples).....	38
3.5.7.3	Solar radiation intensity meter.	39
CHAPTER FOUR.....		41
RESULTS AND DISCUSSIONS		41
4.1	Introduction.....	41
4.2	Heat convective of three models calculation.	41
4.2.1	Heat convective in model with glass /copper tube diameter ratio (1/4).....	42
4.2.2	Heat convective model with glass/copper tube diameter ratio (1/2).....	43
4.2.3	Heat convective model with glass /copper tube diameter ratio (3/4).....	45
4.3	Velocity stream line between nano-fluid and copper tube.....	46
4.4	Efficiency of models with different value of water mass flow rate.	49
4.5	Chosen of optimum model	52
4.6	Experimental results.....	53
4.7	Effect of inlet water temperature on the efficiency.....	55
4.8	Temperatures distribution in the model (1/2)	56
4.9	Temperatures distribution of the water.	56
4.10	Velocity streamline in nano-fluid.	57
4.11	Changing in the distribution of nano-fluid temperature with different inlet water temperature and different mass flow rate.	58
4.11	Cost of the model.	61
CHAPTER FIVE.....		62
CONCLUSIONS AND FUTURE WORK		62
5.1	Conclusion	62
5.2	Future Works.....	63
REFERENCESE.....		64

List of Figures

Figure 2.1: a-Graphic of the flat plate collector. b- (3-D) view of a solar collector filled by nano-fluid[32].	8
Figure 2. 2:Size reduction % for solar collector applying different nano-fluids[33].	9
Figure 2. 3:Efficiency of collector at different volume fraction[34].	10
Figure 2.4: Graphic of volumetric solar collectors[35].	11
Figure 2.5:Thermal conductivity of carbon nanotubes-water in ambient temperature and 60C[37].	12
Figure 2. 6:Change in entropy generation with concentration[38].	13
Figure 2: 7:Graphic of the solar collector[41].	14
Figure 2.8:Graphic of single stage flash (SSF) system[47].	16
Figure 2. 9:Different in water cost and system production as a function of nano-particle. concentration[47].	16
Figure 2.10:Effect of nanoparticle concentration on the collector efficiency[36].	17
Figure 2. 11:Average top temperature of the single tube collector as a function of the nanoparticle concentration[36].	18
Figure 3: 1 a 1 m length a flow water inside copper tube submerged into the nano-fluid.	19
Figure 3: 2 design modeler of tubes.	21
Figure 3: 3 Mesh refinement by assumption of the cell center distance for different mesh sizes.	23
Figure 3: 4 Mesh of crosse section area of model (1/2).	23
Figure 3: 5 Mesh of cross section in Z direction of model (1/2).	24
Figure 3: 6 The Irradiation on External Semi-Transparent External wall.	32
Figure 3: 7 schematic of the losses model.	33
Figure 3: 8 Device Holder	37
Figure 3: 9 water flow meter.	38
Figure 3: 10 Check valve.	38
Figure 3: 11 thermocouples type (K 0.2mm)	39

Figure 3: 12 Arduino Type (SAPPA-103)	39
Figure 3: 13 Interface of measuring solar irradiance application.	40
Figure 4: 1 Temperature distribution, simulated by ANSYS at z = 0.8 m in the model (1/4).....	43
Figure 4: 2 Temperature distribution, simulated by ANSYS at z = 0.8 m in the model (1/2).....	44
Figure 4: 3 Temperature distribution, simulated by ANSYS at z = 0.8 m in the model (3/4).....	46
Figure 4: 4 Streamlines in the plan at z = 0.75 m showing the vortices due to natural convection model (1/4). At 300 k inlet temperature and 0.001kg/s.....	47
Figure 4: 5 Streamlines in the plan at z = 0.75 m showing the vortices due to natural convection model (1/2). At 300 k inlet Temperature and 0.001kg/s.	48
Figure 4: 6 Streamlines in the plan at z = 0.75 m showing the vortices due to natural convection model (3/4). At 300 k inlet Temperature and 0.001kg/s.	48
Figure 4: 7 Efficiency with different mass flow rate of water for three models (1/4),(1/2),(3/4) obtained from ANSYS program simulation.	49
Figure 4: 8 Temperature distribution in interior water for model ¼ with mass flow rate 0.001kg/s	51
Figure 4: 9 Temperature distribution in interior water for model 1/2 with mass flow rate 0.001kg/s.....	51
Figure 4: 10 Temperature distribution in interior water for model 3/4 with mass flow rate 0.001kg/s.....	52
Figure 4: 11 The comparison of theoretical and experimental Efficiency with different mass flow rate of water for model 1/2.	54
Figure 4: 12 Thermal efficiency change with temperature inlet fluid.	55
Figure 4: 13 Temperature distribution along the glass wall of the ratio ½ model.	56
Figure 4: 14 The interface temperature distribution between the inside of copper tube and the flowing water of the ratio ½ models.....	57
Figure 4: 15 Velocity streamline in nano-fluid of the ratio ½ model.	58

Figure 4: 16 Temperature distributions at different value of Z direction with 300K inlet temperature and 0.001 kg/s mass flow rate of water for the ratio $\frac{1}{2}$ model.....	59
Figure 4: 17 Temperature distributions at different value of Z direction 300K inlet temperature and 0.002 kg/s mass flow rate of water for the ratio $\frac{1}{2}$ model.....	59
Figure 4: 18 Temperature distributions at different value of Z direction 305K inlet temperature and 0.001 kg/s mass flow rate of the ratio $\frac{1}{2}$ model.	60
Figure 4: 19 Temperature distributions at different value of Z direction 305K inlet temperature and 0.002 kg/s mass flow rate of the ratio $\frac{1}{2}$ model.	60
Figure 4: 20 Temperature distributions at different value of Z direction 310K inlet temperature and 0.001 kg/s mass flow rate of the ratio $\frac{1}{2}$ model.	60
Figure 4: 21 Temperature distributions at different value of Z direction 310K inlet temperature and 0.002 kg/s mass flow rate of the ratio $\frac{1}{2}$ model.	61

LIST OF TABLES

Table3. 1: Error introduced by assumption of the number of cells center distance for different mesh sizes.....	22
Table3. 2: Properties of base fluid, CuO nanoparticle and 0.055wt% CuO- Engine oil nano-fluid at 300K.	27
Table3. 3: Properties of water at Temperature.....	28
Table3. 4: Properties of copper tube.	28
Table3. 5: Properties of glass tube.	28
Table4. 1: Theoretical results of model $\frac{1}{4}$ obtained from ANSYS program simulation.	50
Table4. 2: Theoretical results of model $\frac{1}{2}$ obtained from ANSYS program simulation.	50
Table4. 3: Theoretical results of model $\frac{3}{4}$ obtained from ANSYS program simulation.	50
Table4. 4: The comparison of Numerical and Experimental of model $\frac{1}{2}$ with inlet water temperature 300k.....	53
Table4. 5: Numerical Results of model $\frac{1}{2}$	54
Table4. 6: Experimental Results of model $\frac{1}{2}$	54

Table4. 7: Experimentally effect of different inlet temperature on the outlet temperature and thermal efficiency ratio ½ models.....	55
--	----

LIST OF SYMBOLS

<i>OD</i>	<i>Ordinary discrete method</i>
<i>NDASCs</i>	<i>Nano-fluid- direct absorption solar collectors</i>
<i>CFD</i>	<i>Computational Fluid Dynamics</i>
<i>RTE</i>	<i>Radiative transfer equation</i>
<i>UDF</i>	<i>User defined function</i>
<i>\dot{m}</i>	<i>Mass flow rate [kg /s]</i>
<i>I_0</i>	<i>Intensity of sun radiation [w /m²]</i>
<i>η</i>	<i>Thermal efficiency [%]</i>
<i>k</i>	<i>Thermal conductivity [W/m K]</i>
<i>p</i>	<i>Nanoparticles</i>
<i>nf</i>	<i>Nano-fluid</i>
<i>bf</i>	<i>Base fluid</i>
<i>ϕ</i>	<i>Volume fraction of Nano-fluid [%]</i>
<i>μ</i>	<i>Dynamic viscosity [Pa.s]</i>
<i>ρ</i>	<i>Density [kg /m³]</i>
<i>C_p</i>	<i>Specific heat capacity [J/(kg K)]</i>
<i>β</i>	<i>Thermal expansion [1/K]</i>
<i>Ke</i>	<i>Extinction coefficient [1/m]</i>
<i>Ka</i>	<i>Absorption coefficient [1/m]</i>
<i>Kt</i>	<i>Scattering coefficient [1/m]</i>
<i>I</i>	<i>Scattered light intensity[w /m²]</i>
<i>Gr</i>	<i>Grashof number [dimensionless]</i>
<i>Re</i>	<i>Reynolds number [dimensionless]</i>
<i>Ra</i>	<i>Rayleigh number [dimensionless]</i>
<i>ΔT</i>	<i>Different in temperature[K]</i>
<i>L</i>	<i>Length [m]</i>
<i>g</i>	<i>Gravitational acceleration [m/s²]</i>
<i>α</i>	<i>Thermal diffusivity [m²/s]</i>
<i>ν</i>	<i>Kinematic viscosity [m²/s]</i>
<i>ρ_0</i>	<i>Constant density of flow[kg /m³]</i>
<i>T₀</i>	<i>Initial temperature [K]</i>
<i>σ</i>	<i>Steven Boltzmann constant [5.6697 x 10⁻⁸ W/(m² K⁴)]</i>
<i>T</i>	<i>Local temperature[K]</i>
<i>Φ</i>	<i>Phase function[dimensionless]</i>
<i>Ω'</i>	<i>Solid angel [dimensionless]</i>
<i>UL</i>	<i>The loss coefficient [W/m² . °C]</i>

h_w	Wind heat transfer coefficient [W/m ² .°C]
Nu	<i>Nusselt number [dimensionless]</i>
K_a	Thermal conductivity of air [W/m K]
T_f	Fluid mean temperature [K]
v	Velocity [m /s]
Q_{loss}	Heat flux to ambient [W/ m ²]
T_{amb}	Ambient temperature [K]
A_s	Surface area of receiver tube [m ²]
T_{sky}	Sky temperature [K]
r	Radius[m]
ϵ_c	Receiver copper emittance [dimensionless]
ϵ_r	Transmittance of glass [dimensionless]
Pr	Prandtl number [dimensionless]
Ra	Rayleigh number [dimensionless]
T_r	Receiver temperature [K]
q'	Convective heat transfer per unit length [W/ m]
K_{eff}	Effective thermal conductivity of nanofluid[W/m K]
L_c	Length scale used in the Rayleigh number [m]

ABSTRACT
EXPERIMENTAL AND CFD ANALYSIS OF NANO-FLUID INSIDE INCLINED
ENCLOSUER

Safaa Rashid SALIH

M.Sc., Department of Mechanical Engineering

Supervisor: Assist. Prof. Dr. Sudantha BALAGE

Co. Supervisor: Assist. Prof. Dr. Amar HAMEED

JULY 2017, 67 pages

Novel configuration for direct absorption solar collector has been developed. In the new configuration, none-circulated nano-fluid absorbs the solar radiation through a glass wall. The absorbed heat is then directly transferred to circulated water flowing inside a copper tube submerged into the nano-fluid enveloped made of glass. Numerical model has been developed for inclined receiver tube which consists of flowing water, nano-fluid annular region and the copper tube which separates the two different fluids. Solar radiation within the nano-fluid is simulated by using ordinary discrete (OD) method in ANSYS FLUENT software. The new configuration has the capability of competing with the traditional solar receiver collectors working on indirect and direct absorption principle. A set of preliminary CFD simulation are performed to obtained the best performing glass-copper size ratio for the solar collector. The ratios of $\frac{1}{4}$, $\frac{1}{2}$ and $\frac{3}{4}$ are investigated using standard copper tubes while the glass tube diameter is fixed at 56 mm. The ratio $\frac{1}{2}$ is found to be the most efficient among the 3 cases. Observations of CFD solutions show that inside the copper tube, water flow rate changes increasingly affecting the efficiency for all size ratios. In nano-fluid region, both of depth of absorption in nano-fluid and characteristic length of natural convection significantly affects the receiver unit efficiency. In size ratio of $\frac{3}{4}$, the insufficient depth of absorption is behind the efficiency shortness. While in size ratio of $\frac{1}{4}$, the insufficient area of convection is behind

the efficiency shortness. The optimum size ratio, which results in sufficient absorption depth and sufficient convection area, appears in the size ratio of 1/2.

The above ratio $\frac{1}{2}$ model is tested experimentally by using a special device and theoretically by ANSYS program with sun radiation intensity of 690 w/m^2 . The different between Experimental and theoretical results are limited between 3.82 and 4.1 as error percentage.

Keywords: Solar collector, direct absorption, nano-fluid, Ordinary discrete method.



ÖZET
EĞİMLİ KAPLAMA İÇERİSİNDEKİ NANO SIVININ DENEYSEL VE CFD
ANALİZİ

Safaa Rashid SALIH

Danışman: Yrd. Doç. Dr. Sudantha BALAGE

Co. Danışman: Yrd. Doç. Dr. Amar HAMEED

Temmuz 2017,67 sayfa

Direkt emilimli solar kolektör için yeni konfigürasyon geliştirilmiştir. Yeni konfigürasyonda, sirküle olmayan nano-sıvılar cam duvar ile solar radyasyonu emmektedir.Emilen ısı ,direkt olarak camla kaplanmış nano-sıvıya daldırılan bakır tüpte bulunan dolaşan akan suya dönüştürülmektedir. Nümerik model, akan su, nano-sıvı yıllık bölge ve iki farklı sıvıyı ayıran bakır tüpten oluşan eğik tüplü alıcı için geliştirilmiştir. Nano-sıvı içerisindeki solar radyasyon ANSYS FLUENT yazılımındaki ordinary dicrete (OD) kullanılarak taklidi yapılmıştır.Yeni konfigürasyon direkt emilim ve direkt olmayan emilim prensibi ile çalışan klasik solar alıcı ile rekabet etme kapasitesine sahiptir. Başlangıç CFD simülasyon takımı,solar kolektör için cam-bakır ölçüm oranının en iyi performansını elde etmek için uygulanmıştır. Cam tüp çapı 56 mm uyarlanarak standart bakır tüpleri kullanılarak $\frac{1}{4}$, $\frac{1}{2}$ ve $\frac{3}{4}$ oranları araştırılmıştır. Diğer 3 durum içerisinde en etkili olanın $\frac{1}{2}$ oranının olduğu ortaya çıkmıştır. CFD solüsyonları üzerinde yapılan gözlemler bakır tüp içerisinde,su akışı oranının tüm ölçü oranların verimini etkileyerek artış şeklinde değiştiğini göstermiştir. Nano-sıvı bölgesinde nano-sıvı emilim derinliği ve doğal konveksiyon uzunluk özelliği önemli şekilde alıcı birim verimliliğini etkilemektedir. $\frac{3}{4}$ ölçü oranında, emilim yetersiz derinliği, verimlilikteki azlığın sonrasında gelmektedir. $\frac{1}{4}$ ölçü oranında ise konveksiyonun yetersiz alanı verimlilikteki azlığın sonrasında gelmektedir. yeterli emilim derinliğin ve yeterli konveksiyon alanın ortaya çıkmasını sağlayan optimum ölçü oranı ise $\frac{1}{2}$ çıkmaktadır.

Üst oran $\frac{1}{2}$ modeli, özel araç deneysel olarak ve 690 w/m^2 yoğunluklu güneş radyasyonlu ANSYS programı teorik olarak test edilmiştir. Deneysel ve teorik sonuçlar arasındaki fark 3.82 ve 4.1 arasındaki hata payıyla sınırlandırılmıştır.

Anahtar kelimeler: Solar kolektör, direk emilim, nano-sıvı, ordinaryüs discrete metodu



CHAPTER ONE

1. INTRODUCTION

1.1 Introduction

Nowadays solar energy is very important sources of renewable energy free and clean, with less environmental contamination. Energy exhaustion increased after industrial revolution clearly, that is lead to intimidation of energy shortage, so scientists search for finding alternative energy sources. Solar energy widely demands to be the very advanced form the energy that belongs to another renewable energy source. By the middle of the 21st century, renewable energy source maybe enough for 60% of the world's electrical market and the rest 40% comes from the fossil fuel[1, 2]. Solar energy is the form of energy that comes from the sun and can be changed to heat and electricity energy. It is a natural result of electromagnetic beam comes "from the sun by the thermonuclear reactions occurring inside its core". The sun has made energy for millions of years. The exploitation of this energy as received attention recently[3, 4]. Some studies have showed that nearly 1000 times of the global energy required maybe produced by solar energy, but just 0.02% of solar energy is currently exploited[5]. The main reason for the big interest in these energy applications is due to the increased the consumption of energy, indicated availability of fuels and ecological significant problems attached with them essentially the carbon dioxide (CO₂) emission. On the other hand, the big increase in the population caused more problem[6]. The sun radiates daily, huge amount of energy and every hour solar beam incident on the earth is bigger than all of human exhausting of energy in a year [7]. While this big amount of available solar energy, near to 80% of the energy used globally still comes from fuels[8]. Recently, one of the future prospects is to decrease global carbon dioxide emissions in 2050 to (75%) of its 1985 level if they can improve and use the renewable energy such as the solar collectors.

In recent years, studies of nano-fluids have increased significantly. These are the fluids containing metal nanoparticles as suspensions. They are studied because of their beneficial properties compared with the pure liquids. Studies have been conducted to determine the physical properties of nano-fluids as desired, and many of the nanoparticles studied, including metal particles[9, 10], and non-metallic particles[11, 12]. In this study, a nano-fluid of CuO suspended in oil is used as the working fluid of a solar collector. (NDASC) uses nano-fluid instead of coated receiver tube. The nanoparticles of the copper oxide have a spherical size of 200 nm and a specific surface area of 80 m² / g[13]. Mass fractionation of the added CuO nanoparticles in the synthetic oil was 0.055 and 0.1 wt%. The surface solar absorber is used in many applications such as the civil application for heating fluids such as water, air. These types of energy absorption system with different configurations and techniques such as flat panel collectors have been widely used. But in low radiation and cold weather condition cannot obtain high energy performance in such conditions. The discharger tubes, containing vacuum space in the confined area between the working fluid tube and the outer cover, reducing the loss of radiation and convection collector can reach the maximum temperature to have high efficiency. So in discharger tubes collector's solar energy is harvested by selective absorber on the upper surface of the tube containing the working fluid. Selective absorber has high absorption in wavelengths of the solar spectrum and less emission of longer wavelength radiation, thus reducing radiation losses[14, 15]. When a low emissivity in these selective of absorbers leads to reduce thermal radiation, major thermal losses at high-temperature values can be absorbed, that is due to the "quadrature of radiation at absorption temperature". In addition, selective surfaces often suffer from high-temperature instability, selective surfaces, they are preferred to be used in environments that have been evacuated, their layers must be stable in the air if the vacuum penetrates [16].In the end, the tubes not discharged have the most losses "due to the non-linear dependence of natural convection on temperature." Direct absorption of the solar spectrum through the working fluid [17] and the addition of gaseous particles [18, 19] is an alternative to surface absorption.

Use the volume of the liquid to absorb Reduces the temperature of the outer surface, which results in less heat loss in relation to the wall absorption scheme.

Recently, Tiyagi et al [20].The effect of different parameters on collector efficiency type (NDASC), as well as Otanikar et al[21, 22]. The two sides studied both experimentally and numerically the effects of nano-fluids at different concentrations and for many types (graphite and silver, carbon nanotubes) on the work of a small channel absorbing direct solar absorption energy. The physical properties of CuO, showing that CuO changed the optical properties of oil at different concentrations.

1.2 Problem Statement

Nano-fluid is the fluid containing nanoparticles mixed in them to be as suspension. The suspended nonmetallic or metallic nanoparticles change the thermal characteristics and transport properties of the fluid. Nano-fluids are the new generation of heat transfer fluid for different application such as in automotive and industrial applications because of their good thermal efficiency. The above was discovered accidentally at Argonne National Laboratory of USA by Choi in 1995 [23], that showed that the traditional fluid thermal efficiency could be attracting attention refinement by using nanoparticles. Nano-fluids can be used for large forms of engineering applications such as, thermal management of electronics, transportation, medical, defense, nuclear, and space, [24]. One of the keys issues of energy saving and compact designs is heat transfer improvement in the solar collector. Solar energy used in applications like, chemical processing, electricity generation and heating due to its nonpolluting nature and renewable. Generally, solar water heating systems have two parts: a storage tank and the solar collector (tubes or flat plate). The most conventional solar collector is called a flat plate collector but these have low efficiency. There are a lot of solutions introduced to rise the efficiency of the solar water heater [25].

The thermal conductivity of the fluid conveying thermal heat was improved by using nano-fluid in the literature, but still, heat exchange needs more improvement by enhancing the fluid thermal conductivity or by improving the configuration to boost heat transfer. the mean objective of the research to increase of solar energy harvesting by reduction of thermal resistance in the medium fluid. New configuration will be submitted for heat transmitting in inclined pipes from nano-fluid to heating system.

1.3 Thesis Objective

Solar collectors' uses nano-fluid as a working fluid has a higher performance compared to the conventional solar collectors. Recently nano-fluid has found attention in more applications that required effective and quick heat transfer for example, cooling of microchips, industrial applications, etc. However, the dissimilarity between the traditional heat transfer and the solar thermal applications makes the advantage of the nano particles unclear. Nano-fluid scatters and absorbs a lot of the solar beam passing through it. A solar collector that use black plate absorber to collect the beam's heat energy and then transforms it to the working fluid flowing in tubes fixed within. Because of the (Differentness determinations have been found with these arrangements and replacement significances have been studied). Through these, use of nanoparticles mixed with the base fluid is the subject of research.

There are two main goals in this study. The first is to increase the overall efficiency of the solar collector by using non circulated nano-fluid. The second is to use the minimum amount of nano-fluid in order to decrease the cost of the system. CFD simulations and an experimental setup of solar collectors is made.

1.4 Organization of the Thesis

Chapter 1: Includes introduction, thesis objective, and problem statement.

Chapter 2: includes the previous studies about solar collectors that work by using nano-fluid as a work fluid with different size, type and concentration of nanoparticles.

Chapter 3: includes the methodology of CFD and experimental of thesis.

Chapter 4: includes the results of CFD and experimental work supported with tables and charts.

Chapter 5: includes the Conclusion and Future work.

CHAPTER TWO

LITERATURE REVIEW

2.1 Introduction

Renewable energy is the main entity for developing the economy of countries. Moreover, fossil fuel facing the biggest part of the energy consumption is intimidating and their availability is reducing continuously. Recently, solar energy collectors play a principle part in the produce of energy by changing solar energy to electricity or heat energy. The environment protection and doubt over future energy requirements, solar energy is a good substitution aL form although it is more expensive operational. Heat transfer improvement in solar collectors is the important issues in compact designs and energy-saving. A change the working fluid with nano-fluid to enhance heat transfer characteristic of the base fluid is one of the effective technique. Recently, most of the researchers have become attentive in the use of nano-fluid in a combination of different solar devices, solar cooling systems, solar collectors, solar cells, solar absorption refrigeration devices, and water heaters due to the higher thermal conductivity of nano-fluid and the irradiative properties of metallic nanoparticle in a base fluid. The selection convenient nano-fluid in solar applications is the main issue. The effectiveness of nano-fluids, for example, absorber work fluid in a solar collector depends on the kind of base fluid and metallic nanoparticles, the concentration of nanoparticles, irradiative properties of nano-fluid, temperature of the fluid, size nanoparticles, stability of the nano-fluid and pH values, [26]. There is only a few precedent research have discussed the ability of nano-fluids to improve the efficiency of solar collectors [27, 28]. In this thesis, we try to increase of solar energy harvesting by reduction of thermal resistance in the medium fluid. The new configuration will be submitted for heat transmitting in inclined pipes from nano-fluid to heating system.

2.2 Literature review of solar collectors based nano-fluid in the recent years.

1. Qiao L., et al. [29]. Experimentally demonstrated that the radiation absorption of Aluminum nano-fluids is higher than Al_2O_3 nano-fluids. Base-fluids used is water. The case is different due to different in an optical property of the Al_2O_3 . Low radiation absorption of Al_2O_3 nanoparticle does not effect on greatly on localized convection of heat transfer to the fluid. Used of nano-fluid type Al_2O_3 based water for cooling was studied for the silicon solar collector by using the method of the finite element by Mehdaoui R et al. [30]. They assumed the panel solar collector as a slope cavity in an angle of 30 degrees. Application of Nano-fluids increased the value of the nusselt number and average cooling. They improved (27%) in the rate of heat transfer with 10% weight fraction of Al_2O_3 -water nano-fluid with $\text{Re} = 5$.

2. Wang C et al. [31] calculated the efficiency of the direct absorber solar collector DASC with nano-fluids by using the two-dimensional model of the radiation transfer equations RTE of particles medium and combination conduction and convection heat transport equation. Nano-fluid flows in the horizontal direction from left to right with steady state assumption. Solar collector was covered by a glass plate. The solar radiation simulation was used for validating this model. They used nanoparticles of SiO_2 , Al_2O_3 , TiO_2 Cu, Ag, oscillating graphite and carbon nanotubes CNTs by dispersing them with synthetic oil as a base fluid. The results showed that use of nano-fluids in solar collectors lead to increase in the efficiency of collector and outlet temperature. They also demonstrated that the efficiency of most nano-fluids are almost similar and higher than that of base fluid (oil), except for Tio_2 .

3. Mojumder S et al. [32] perform a numerically for a flat plate solar collector which uses nano-fluid by A Galerkin weighted finite element method code was used for a wide range of Grashof numbers (Gr). The low corrugated plate is at a high temperature and the side walls of the triangular enclosure are at a low temperature Figure (2.1). It is assumed that both nanoparticles and fluid phase are in thermal equilibrium and no slip between them. Nano-fluid is incompressible and Newtonian, and

flow is unsteady and laminar. Considered that constant properties for nano-fluid except for density divergence in the buoyancy forces limited by using the Boussinesq approximation. However, they have not determined the diameters of particles. They provide high value of Grashof number and concentration proved higher heat transfer by conduction and convection. The results proved that for Grashof number = 106 with 10% concentration lead to a 24.28% enhancement when use copper nano-particle. When the Grashof numbers number, is lower conduction is the primary means of the heat transfer for any concentration value. The study proved that the heat transfer by convection performance is the best when the concentration is 0.08% or 0.05%. This paper also showed that Cu/water nano-fluid is the better than others nano-fluids for the increase rate of heat transfer.

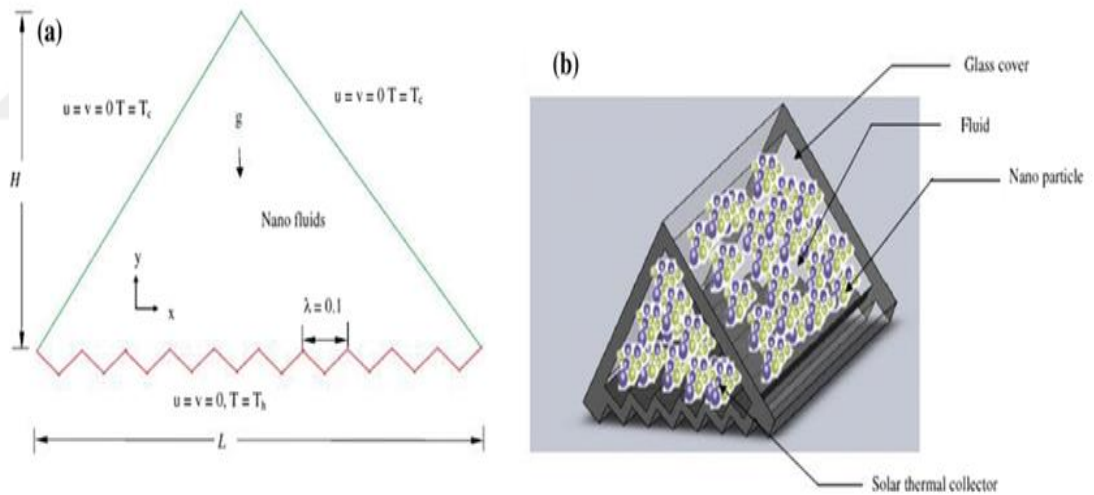


Figure 2.1: a-Graphic of the flat plate collector. b- (3-D) view of a solar collector filled by nano-fluid[32].

4.Saidur R et al. [33]achieved the contribution size reduction of nano-fluid solar collectors and thermal performance to assessment the price reserve. The conclusion of this study defined that performance of solar collector used nano-fluid as a working fluid can calculate in the function of specific heat, mass flow rates and density of nano-fluid. They proved that low specific heat and high density of nano-fluid gives higher

performance than the water and may decrease the area of collector near to 21.1%, 25%, 21.5%, 20.1% with AL₂O₃, TiO₂, SiO₂, and CuO nano-fluid, Figure (2.2). So, it will decrease the weight, price and energy of manufactured the collectors.

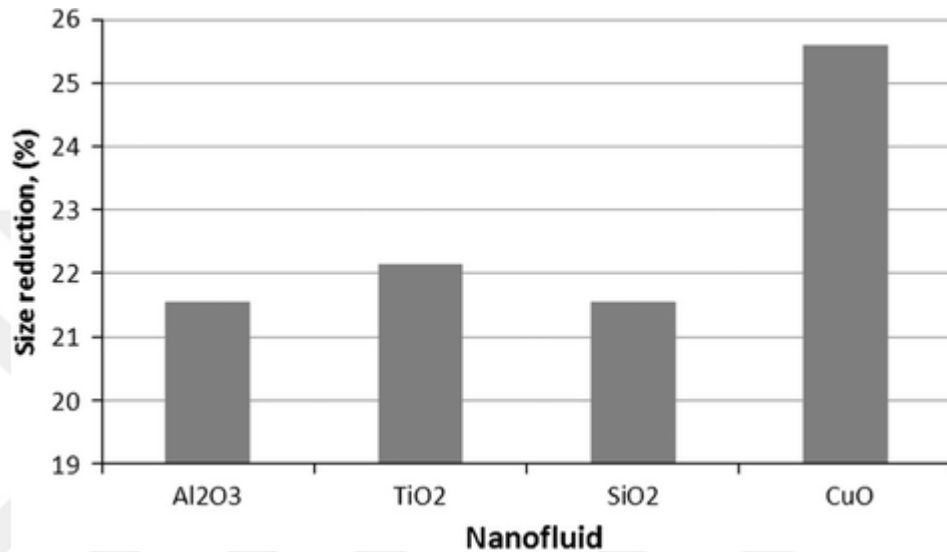


Figure 2. 2:Size reduction % for solar collector applying different nano-fluids[33].

5.Nasrin R et al. [34]investigated the effects of volume fraction of nanoparticles ($\phi = 0, 1, 3, 5$ and 7%) and the Reynolds number ($Re = 200, 400, 600, 800$ and 1000) on the distribution of temperature, collector efficiency, and entropy generation rate. The kind of nano-fluid used incompressible type water-Cu with the laminar condition. Their results are shown below:-

a- Increasing the nanoparticles concentration raises the fluid viscosity reducing the Reynolds number. The reduction of Reynolds number leads to reduced heat transfer.

b- It is necessary to choose the best concentration of nano-particles for base fluids.

c- Efficiency of solar collectors may be increased to twice by using Cu/water and Ag/water nano-fluids with the volume fraction of 3% see Figure 2.3.

d- Enhanced the entropy generation up to volume fraction ($\phi = 3\%$) after this value, the addition of nano-particles does not make changes in the generation of entropy.

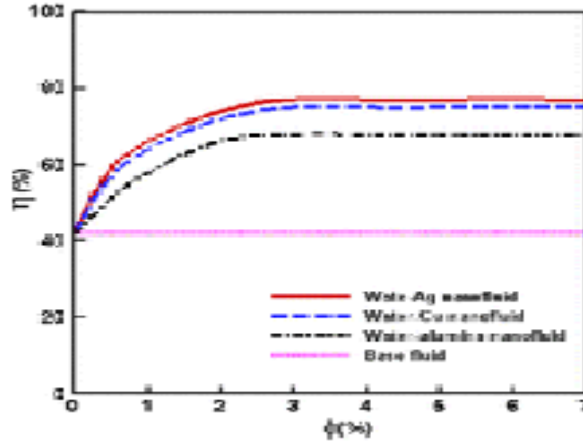


Figure 2. 3:Efficiency of collector at different volume fraction[34].

6.Asnaghi, A. et al. [35]studied numerically the effect of nano-fluid on the efficiency of the solar collector (Figure 2.4) with different volume fractions and diameter of carbon nano-particles. They noted that in the infrared range, optical properties of the water are dominated, however in the visible ranges that extinction coefficient value is dependent on the volume fraction of nano-fluid. Extinction coefficient can calculate by sum the scattering and absorption coefficients in this study. The study proved that efficiency of nano-fluid solar collector increases near to (88%) compared with the solar collector using water with the 313 Kinlet temperature of nano-fluid.

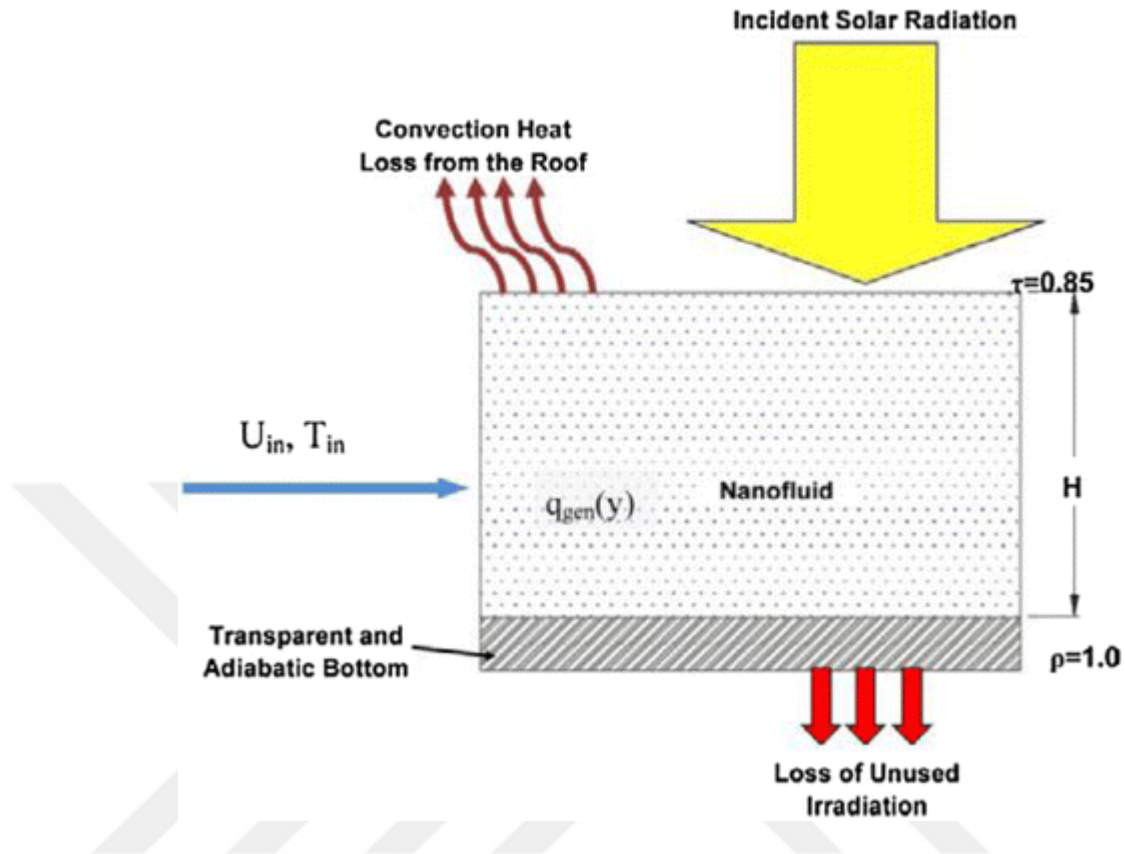


Figure 2.4: Graphic of volumetric solar collectors[35].

7.Mendoza OSH et al. [36]studied nanoparticles of silver as direct absorbers of solar collector applications. They showed that nanoparticle increases the stored energy by 144, 93 and 52% for the silver particles of volume fraction 6.5, 3.25 and 1.62 particle per million ppm respectively .So They found the effect of the volume fraction of specific absorption value just discernible at the initial heating. They demonstrated that the decreases in specific absorption value at the high concentration of 650 ppm may be because of:

a-The conglomerate of metallic nano particles, that lead to reducing the sunlight intensity into the nano-fluid because of the nano-particles deposited on the surface.

b- The deferens in the absorpion efficiency of these conglomerates at the various depth of nano-fluids.

8. AkhavanBahabadi MA et al. [37] showed that water based carbon nanotubes (CNT) with the diameter 10 nm and length 5-10 μm , has high stability as an absorber nano-fluid for low temperature in a NDASC. The CNT considerably improved the thermal conductivity of base fluid and decreases the transmittance see (Figure 2.5). They advise the uses of these types of nan-fluids to absorb the spectrum of the sun directly. In their research, CNTs was dispersed into the water by an ultrasonic instrument with the volume fractions less than 150 ppm. Higher concentrations produced a black solution which light was not able to pass through.

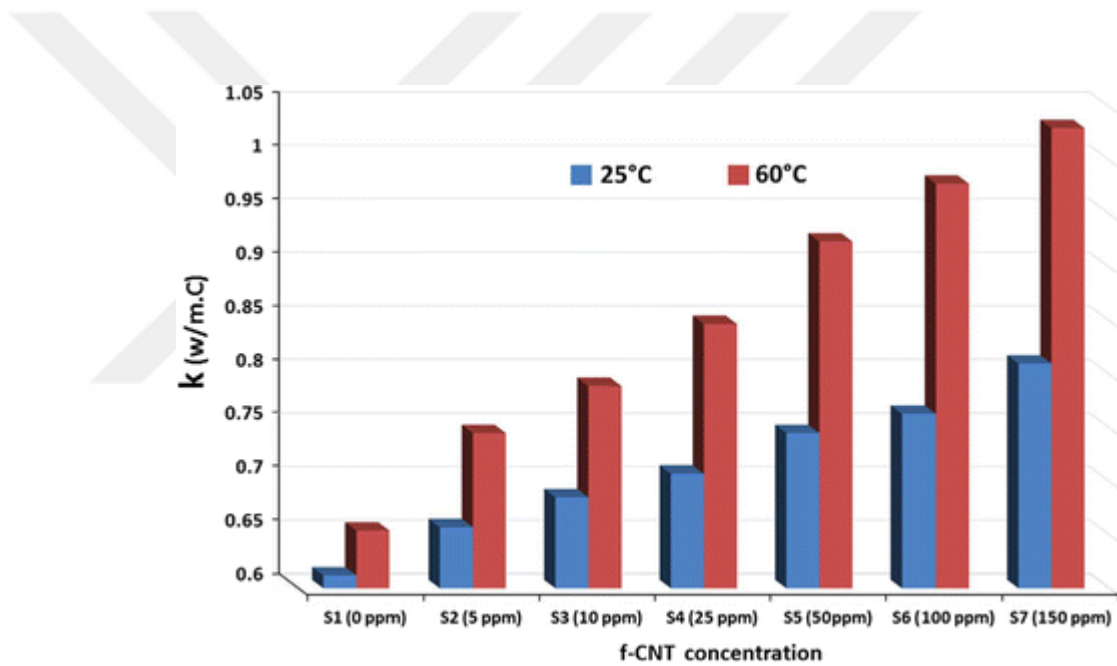


Figure 2.5: Thermal conductivity of carbon nanotubes-water in ambient temperature and 60C[37].

9. Saidur R et al. [38] showed that single wall carbon nanotubes (SWCNT) based nano-fluid in the flat plate type solar collector has a lower generation of entropy compared with the nano-fluids consists of TiO_2 , SiO_2 and Al_2O_3 nano-particles with same base fluid see (Figure 2.6). They attributed the decrease of the entropy generation to the increase in heat flux on the absorber plate due to the nanoparticles addition. It was observed that the single wall carbon nanotubes nano-fluids could enhance the heat

transfer coefficient hc about 15.33% and reduce the entropy generation by about 4.34%. Also It had a low resistance in the pumping power about 1.2%.

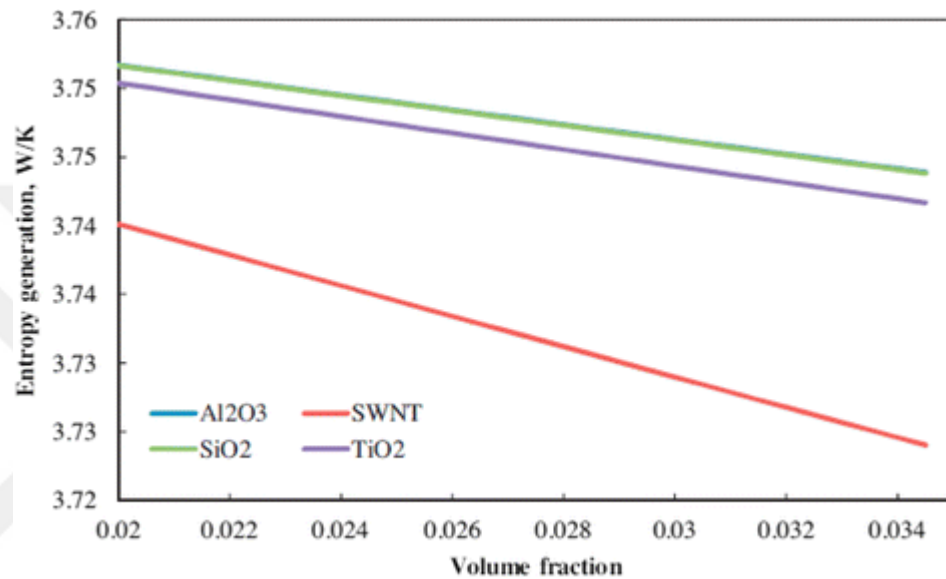


Figure 2. 6:Change in entropy generation with concentration[38].

10.Wang Y et al. [39]used the composites of carbon nanotubes, SiO₂, poly ethylene glycol (PEG), multi wall carbon nano tubes MWCNTs, inorganic SiO₂ and poly ethylene glycol PEG. This composite has a high thermal conductivity compared with conventional phase change materials due to the high thermal conductivity of multi wall carbon nanotubes MWCNTs. The results proved that SiO₂/MWCNT/ PEG components can enhance the performance of solar energy applications.

11.Meng TC et al. [40]studied the effect of many various on the performance of a low temperature NDASC used aluminum nanoparticles based water. The advantage of using low temperature collectors that the solar systems can be simple and not expensive. Additionally, there are a number of working fluids suitable to low-temperature operation. Commonly used base liquids are water, oil, and ethylene glycol. They considered the effects of scattering and absorption of the solar radiation through the

nano-fluid by using the Radiative Transfer Equation (RTE). To evaluate the nano-fluid spectral extinction coefficient, that is the sum of absorption and scattering coefficients, they used the optical properties of the nanoparticles and fluid separately. The results showed that water based aluminum nano-fluid of 1% concentration enhance the absorption of solar radiation significantly. Their results showed that the effect of the size of particles on the optical properties of nano-fluid is minimum. So they showed that extinction coefficient is linearly proportional to the concentration.

12. Parvin S et al. [41] Numerically demonstrated the effect of Prandtl number (Pr) on flow velocity fields, temperature, radiative and convective heat transfer rates of the fluids in a solar collector. They used Al_2O_3 /water nano-fluid (see Figure 2.7). They showed that increasing Pr from 1.73 to 6.62, lead to an enhancement of the convection heat transfer by 18% to 26% respectively for the base fluid and nano-fluid whereas radiation improved by about 8%.

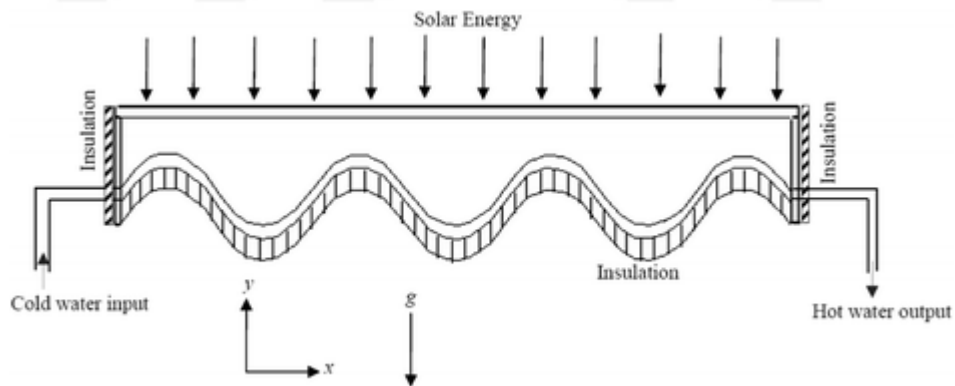


Figure 2: 7:Graphic of the solar collector[41].

13. Rabilloud D et al. [42] used four nano-fluids by suspending Multi Wall Carbon Nano-tubes in propylene glycol, ethylene glycol and water by the help of an ultrasonic bath. They tested both the high-temperature and long term stable of CNTs and nano-fluids for using in direct solar collectors. In this study plasma treatment is used to vary the surface of multi wall carbon nanotubes to enhance the dispersion through the base

liquids. This work mentioned a quantitative demonstration of the high- temperature stability of ethylene glycol with multi wall carbon nanotubes MWCNT nano-fluids for solar collectors.

14. Zhao F et al. [43] Experimental showed that the solar collector completed by open thermo syphon has a better performance collecting and its efficiency may be enhanced by using working fluid type CuO based water nano-fluid as well. Results proved that the minimum and maximum values of the collecting performance of the solar collector with open thermo syphon using nano-fluids increased 6.6% and 12.4%.

15. Veysi F et al. [44, 45] experimentally investigated the effect of Al₂O₃ 15 nm and Multi Wall Carbon Nano-tubes size 10-30 nm based water nano-fluid on the thermal efficiency of a solar collector. The concentration of nano-particles (0.2 and 0.4%) weight fraction. Their findings showed that the surfactant presence in the nano-fluid extremely affects solar collector's efficiency.

16. El-Said EMS et al. [47] made a unit for water purification coupled with (Cu-water) nano-fluid-based a flat plate solar collector as a heat source Figure 2.8. The collector consists of a flashing chamber, a solar water heater, and a mixing tank plus a condenser and a helical heat exchanger. The purification process depends on the water evaporation in a vacuum. The evaporated water then condensed to get pure water. They showed that the volume fraction is very important to decrease the cost and increase the pure water production. Their results showed that can decrease the cost of water from 16.43 \$ /cm to 11.68 \$ /cm with volume fraction 5%, Figure 2.9.

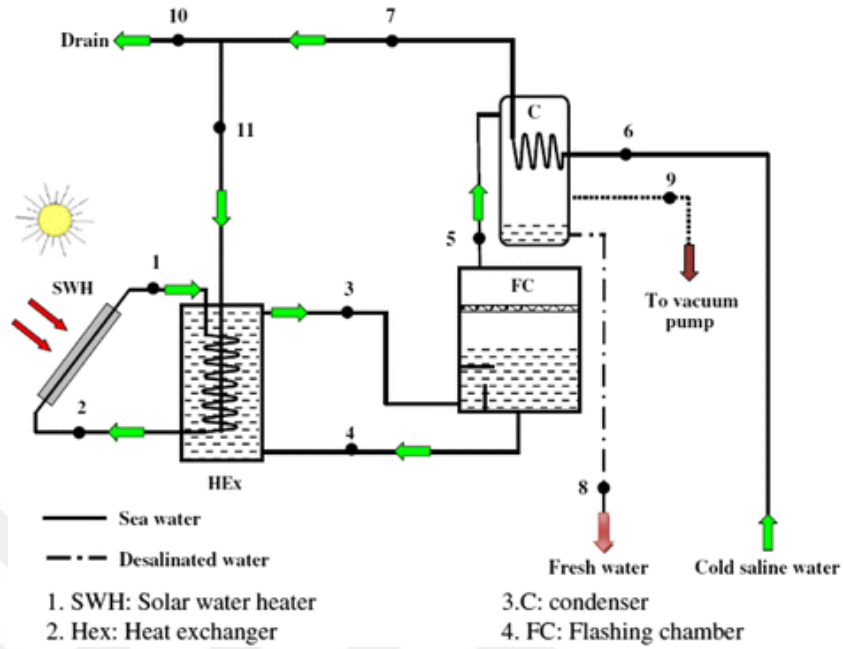


Figure 2.8: Graphic of single stage flash (SSF) system[47].

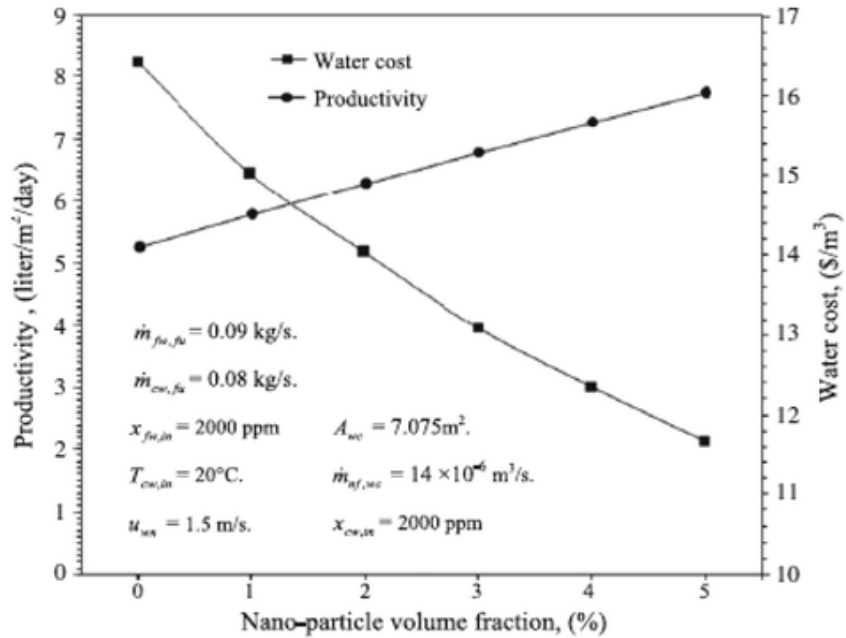


Figure 2. 9: Different in water cost and system production as a function of nano-particle concentration[47].

17.A Moradia et al. [36] numerically investigated nano-fluid direct absorption solar collector using single wall carbon nanohorn based nano-fluids have been as a function of the nanoparticles concentration and for ethylene glycol and water base fluids. Values of optical properties of nano-fluids have been considered with the fluid dynamics simulation, with considered both the heat transfer and optical ray tracing (3d) analysis. The single glass tube collector operating with a nano-fluid in the presence of both forced and natural convection losses has been considered. Their results showed that the efficiency of solar collector depend on the nanoparticle concentration in the nano-fluid, because of the higher collector surface temperature can obtained by increasing the volume fraction. As for the effect of the base fluid, they proved that glycol show higher outlet temperature, while water based nano-fluid produce higher values of efficiency, see figures (2.10, 2.11)

Their results help to limit the appropriate base fluid for various operating conditions. Their simulations explained that the use of SWCNHs based nano-fluids give a high-temperature distribution within the fluid having the same maximum inside the same fluid, consequently making such nano-fluid DASC very competitive when compared with the conventional solar collectors using black tubes, where the higher temperature value is always attained at the surface.

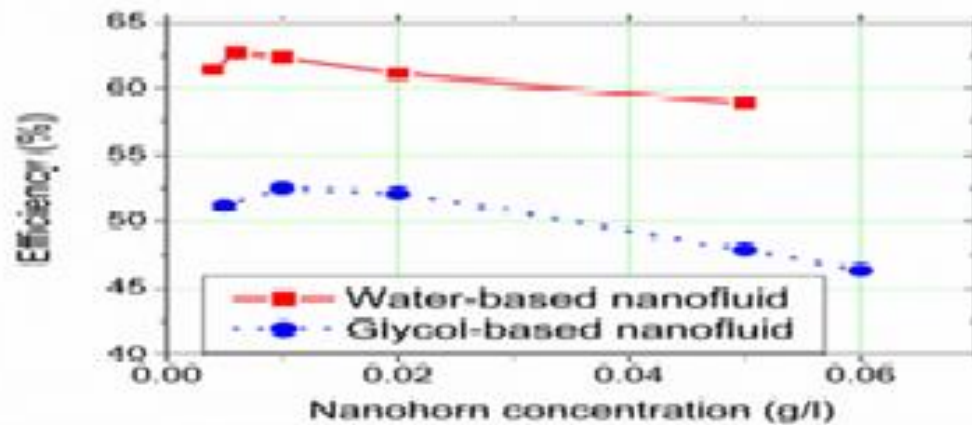


Figure 2.10: Effect of nanoparticle concentration on the collector efficiency[36].

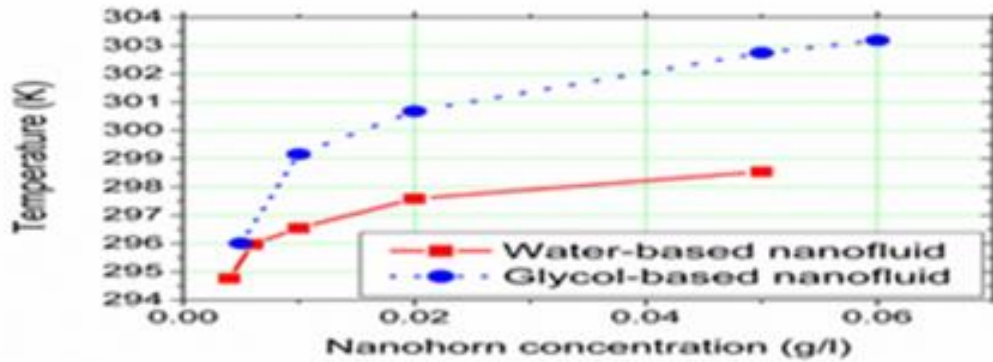


Figure 2. 11: Average top temperature of the single tube collector as a function of the nanoparticle concentration[36].

2.3 Conclusion of literature review.

A review of previous researches shows that there are some of the theoretical and experimental studies trying to increase solar energy harvesting. In all cases Nano tubes or nanoparticles are found to be beneficial. Increase prandtl number and the increase Reynolds number improve the heat transfer. The addition of nanoparticle increases the prandtl number, but decreases the Reynolds number. This study tries to increase solar energy harvesting by reduction of overall thermal resistance.

CHAPTER THREE

Simulation And Experimental of System

3.1 Introduction.

In this study, a three-dimensional numerical simulation of the nano-fluid based solar receiver is performed. The absorbed heat directly transfers to circulated water flowing inside copper tube submerged into the nano-fluid, see figure 3.1a,b. The study was conducted by using the ANSYS FLUENT software, for 3 models, glass-to-copper tube diameter ratio of 1/4, 1/2, and 3/4, combined with ANSYS UDF developed in order to include natural losses in the collector.

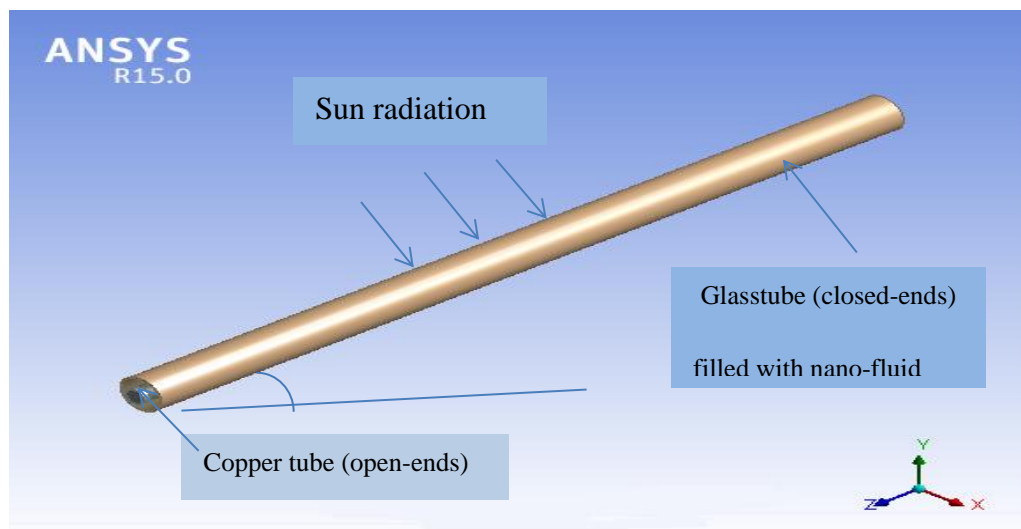


Figure 3. 1. (a) 1 m length a flow water inside copper tube submerged into the nano-fluid.

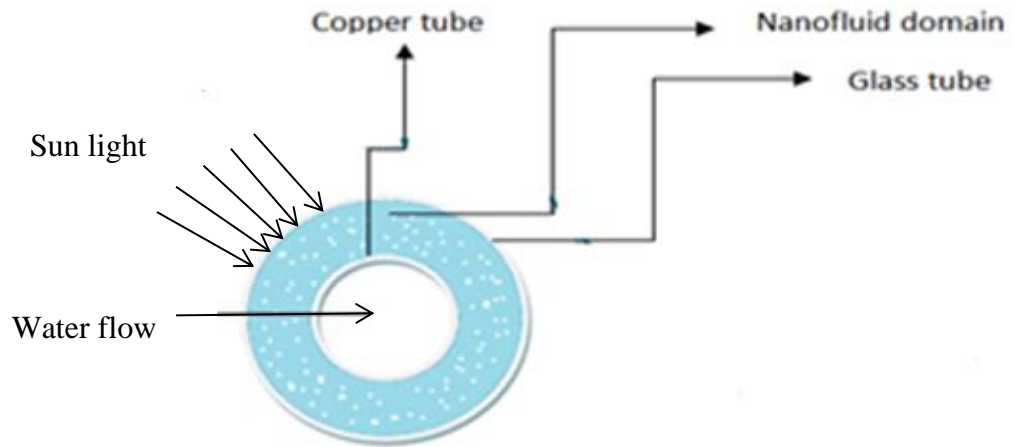


Figure 3.1: (b) Cross section area flow water inside copper tube submerged into the nano-fluid.

The simulation in ANSYS FLUENT software R15.0 is carried out under the following assumptions.

- 1- Steady state conditions.
- 2- The fluids are in one phase.
- 3- The density of water flowing inside the copper tube is constant.

3.2 Design of models

In this part, a three different dimension models with size ratios 1/4, 1/2, 3/4 were designed in 3-dimension with different dimensions of inner copper tubes diameters 11.75, 22 and 35 mm, 3 mm in thickness and 1m in length. The copper tubes submerged in a constant glass tube internal diameter 51 mm and 2.25 mm in thickness with length 1.05m filled with nano-fluid for all models as shown in Figure3.2.

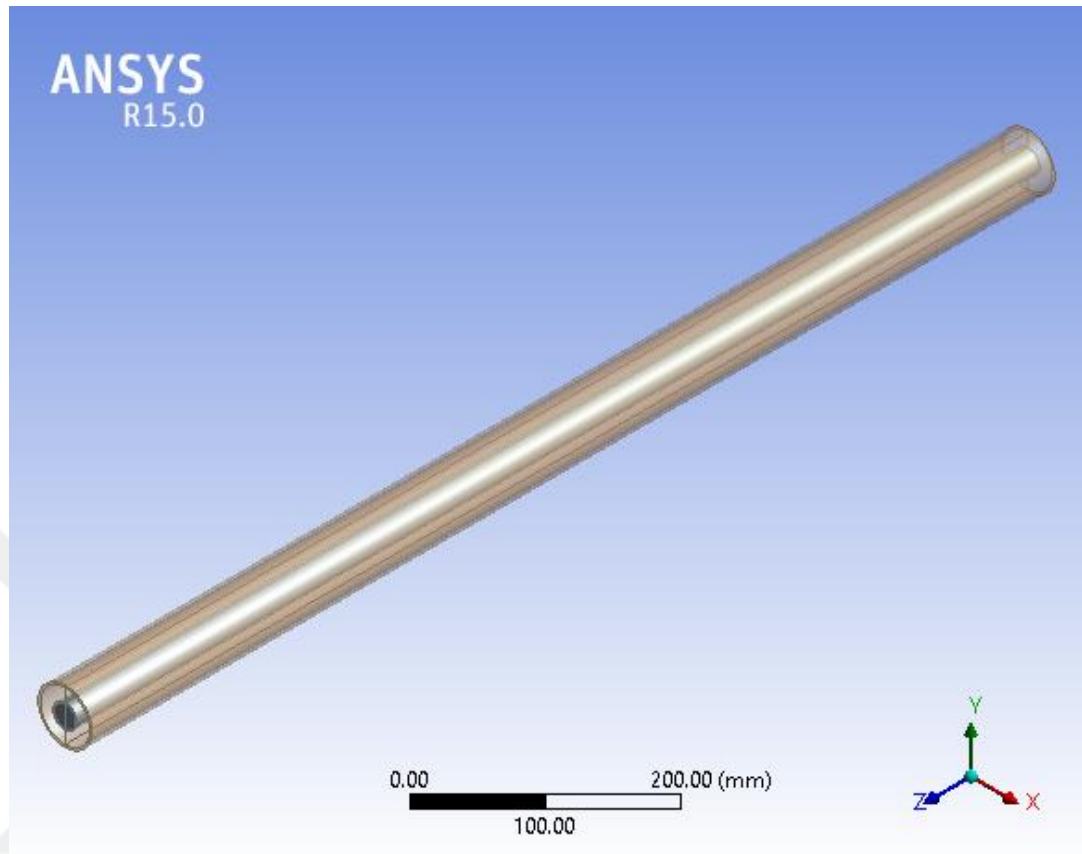


Figure 3. 2: Design modeler of tubes.

3.3 Grid Generation

In this part, Multi-Zone method with number of division for all diameters, lengths of tubes, nano-fluid and water was chosen to decrease the error percentage of the results. Mesh refinement was investigated for 6 different meshes of the model 1/2 with the mass flow rate of water 0.002 kg/s , intensity of sun radiation 877 W/m^2 and compared. We find that for a number of divisions of each diameter 360 divisions, and for each length 500 divisions the error is fairly low 0.11%, as seen in table 3.1 and figures 3.3, 3.4, 3.5 below.

Table3.1: Error introduced by assumption of the number of cells center distance for different mesh sizes.

No	ΔT water (k)	Efficiency %	Total number of cells	Error %
1	7.2131	39.24	2812113	7.5
2	7.8	42.432	4064112	7.14
3	8.4	45.7	6673320	1.06
4	8.49	46.18	8605677	0.83
5	8.561	46.57	9329622	0.11
6	8.57	46.6	9935054	

$$\text{Efficiency} = \frac{\dot{m} C_p \Delta T}{A_s \cdot I} * 100\%$$

$$\text{Error} = \frac{\eta_n - \eta_{n-1}}{\eta_n} * 100\%$$

Where:-

\dot{m} is the mass flow rate of water in kg/s

ΔT is the different between inlet and outlet water temperature in K.

I is the sun radiation intensity in W/m².

A_s is the surface area of glass tube.

C_p is the specific heat of water in J/(kg K)

η_n is the Subsequent thermal efficiency %.

η_{n-1} is the Previous thermal efficiency %.

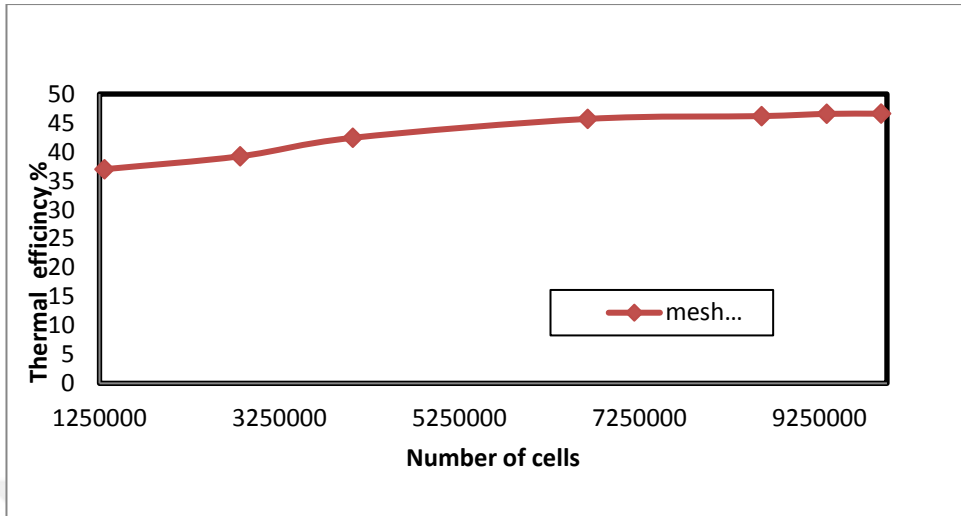


Figure 3.3: Mesh refinement by assumption of the cell center distance for different mesh sizes.

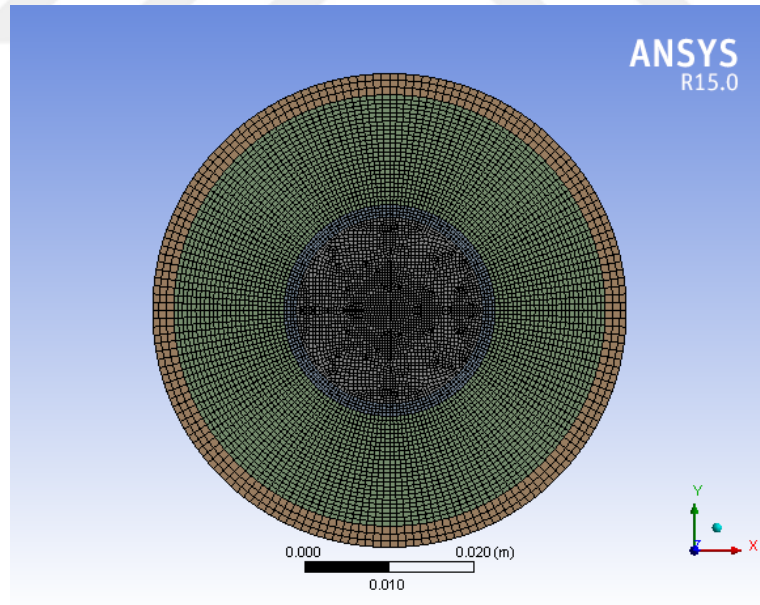


Figure 3. 4: Mesh of cross section area of model (1/2).

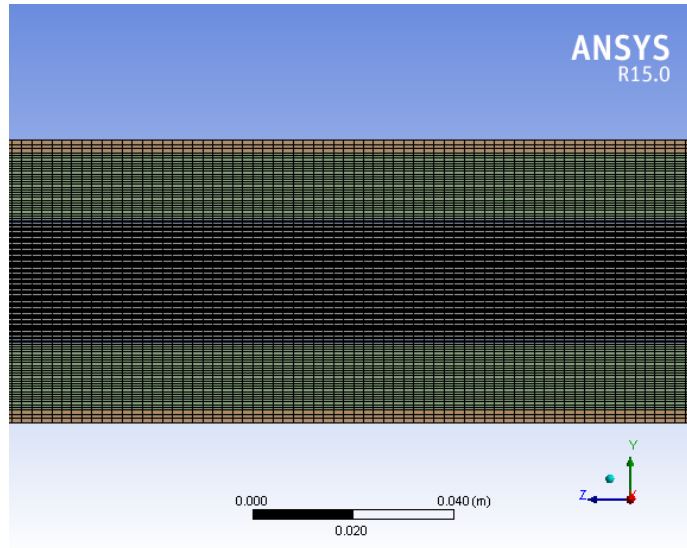


Figure 3. 5: Mesh of cross section in Z direction of model (1/2).

3.4 FLUENT modeling methodology

The main steps of simulation in the ANSYS FLUENT software are, specifying and outlining of the model's geometry according to the main design consideration. When the tool of CFD analysis depends on the finite volume model, the mesh of the model is an important second step of the solutions. The setting of general simulation model should be done when the radiation solar load model and energy equation take place. Determination the model orientation altitude, latitude, and time zone. Identify model used material kinds, boundary conditions, and properties. Finally, setup the solution and post process are completed.

3.4.1 Inclined Angle.

The amount of thermal energy produced by solar collectors depends largely on the value of inclined angle, so it must be correctly identified to increase the rates of solar radiation gained. Therefore, the ideal angle of the solar collectors for the countries was determined monthly and annually by accurately identifying their locations based on the Google Earth program[48].

3.4.2. Properties of materials used in simulation.

In this research, none-circulated nano-fluid absorbs solar radiation through glass wall was chosen. The absorbed heat directly transfers to circulated water flowing inside copper tube submerged into the nano-fluid, nano-fluid annular region and the copper tube which separates the two different fluids.

3.4.2.1 Calculation of nano-fluid properties.

In this research, copper oxide CuO based engine oil nano-fluids was chosen and used as a working fluid for the solar collector type NDASC. A Scanning Electron Microscope SEM [53].image shows the spherical CuO nano-particles having the size of 200 nm. Nano-particles have the specific surface area (80m²/g). The volume fraction concentration of the CuO nano-particles in the base fluid is 0.055 %. The properties of the CuO nano-particles, engine oil type 5W30 and nano-fluid shown in table 3.2. [53]

3.4.2.1.1 Thermal Conductivity of nano-fluid in W•(m•K)⁻¹.

Thermal conductivity of nano-fluid can calculate by the Equation 3.1 shown below for the spherical metallic nano-particles.

$$k_{nf} = \frac{k_p + 2k_{bf} + 2\varphi(k_p - k_{bf})}{k_p + 2k_{bf} - \varphi(k_p - k_{bf})} k_{bf} \dots \dots \dots 3.1$$

Where:

k_p is the thermal conductivity of nanoparticles, k_{bf} is the thermal conductivity of the base fluid, k_{nf} is the thermal conductivity of nano-fluid, all quantities in W•(m•K)⁻¹

[49].

3.4.2.1.2 Dynamic viscosity of nano-fluid in (Pa•s).

The viscosity of nano-fluid of nano-fluid can calculate by the Equation 3.2 shown below for the spherical metallic nano-particles.

$$\mu_{nf} = (1 + 2.5 \varphi + 6.2\varphi^2)\mu_{bf} \dots\dots\dots 3.2$$

[49].

Where:

μ_{nf} is the dynamic viscosity of the nano-fluid, μ_{bf} is the dynamic viscosity of the base fluid in Pa•s, φ is the volume fraction on nano particles to base fluid%.

3.4.2.1.3 Specific heat and density of nano-fluid in J•(kg•K)⁻¹ and (kg•m⁻³).

Specific heat and density of nano-fluid can calculate by the Equations 3.3,3.4 shown below for the spherical metallic nano-particles.

$$\rho_{nf} = (1 - \varphi)\rho_{bf} + \varphi\rho_p \dots\dots\dots 3.3$$

$$(\rho C_p)_{nf} = (1 - \varphi)(\rho C_p)_{bf} + \varphi(\rho C_p)_p \dots\dots\dots 3.4$$

[49].

Where:

ρ_{nf} is the density of the nano-fluid, ρ_{bf} is the density of the base fluid, ρ_p is the density of the nanoparticles, all quantities in kg/m³.

C_{pnf} is the specific heat of the nano-fluid, C_{pnp} is the specific heat of the nano particle, $C_p bf$ is the specific heat of the base fluid, all quantities in J•(kg•K)⁻¹

3.4.2.1.4 Coefficient of volume expansion of the nano-fluid in (1/k).

The coefficient of volume expansion of the nano-fluid can calculate by the Equation 3.5 shown below for spherical metallic nano-particles.

$$\beta_{nf} = \frac{(1 - \varphi)\rho_f\beta_f + \varphi\rho_p\beta_p}{\rho_{nf}} \dots\dots\dots 3.5$$

[50].

Where:

β_{nf} is the thermal expansion the nano-fluid, β_p is the thermal expansion the nano particles, β_f is the thermal expansion the base fluid, all quantities in K^{-1} .

3.4.2.1.5 Absorption and scattering coefficients of the nano-fluid in (1/m).

Absorption and scattering coefficients are connected each other by the extinction coefficient. Lambert-Beer in equation 3.6 gives the relationship between the light extinction after a path length (s) through the medium showing both scattering and absorption effects [51, 52]:

$$I = I_0 * e^{(-ke*s)} \dots\dots\dots 3.6$$

Were:

I is the Scattered light intensity, I_0 is the Intensity of sun radiation in w/m^2 , s is the path length in m, ke is the extinction coefficient in 1/m.

Note: Ke The extinction coefficient Ke , can give by the sum of the scattering coefficient K_t and absorption coefficient K_a in equation 3.7 shown below [52]:

$$K_e = K_a + K_t \dots\dots\dots 3.7$$

Table3.2: Properties of base fluid, CuO nanoparticle and 0.055wt% CuO- Engine oil nano-fluid at 300K.

Parameters	Cp	P	k	μ	Ka	Kt	β
Unit	$J \cdot (kg \cdot K)^{-1}$	$kg \cdot m^{-3}$	$W \cdot (m \cdot K)^{-1}$	$Pa \cdot s$	m^{-1}	m^{-1}	K^{-1}
CuOnanoparticles	475	6300	33	-	-	-	$1.8 \cdot 10^{-5}$
Engine oil5w30	1900	840	0.14	0.063	2	2	$7 \cdot 10^{-4}$
Nano-fluid	1899.2	843	0.14022	0.0630 8	103	401	0.00069962

3.4.2.2 Properties of liquid water

Physical and thermal properties of the liquid water flowing can list in Table 3.3 shown below at Temperature 300-350K.

Table3.3: Properties of water at Temperature.

parameters	temperature	ρ	Cp	k	μ
Unit	K	Kg.m ⁻³	J.(kg.K) ⁻¹	W.(m.K) ⁻¹	Pa.s
Water	300	997	4179	0.613	8.55x10 ⁻⁴
	325	987	4182	0.645	5.28x10 ⁻⁴
	350	973	4195	0.668	3.65x10 ⁻⁴

3.4.2.3 Properties of copper tube.

Physical properties of the copper can list in Table 3.4 shown below.

Table3.4: Properties of copper tube.

Parameters	Cp	P	Emissivity ϵ_c	k
unit	J•(kg•K) ⁻¹	kg•m ⁻³	-	W•(m•K) ⁻¹
value	381	8978	0.07	387.6

3.4.2.4 Properties of glass tube.

Physical properties of the glass tube (Pyrex) can list in Table 3.5 shown below.

Table3.5: Properties of glass tube.

Parameters	Cp	ρ	k	Emissivity ϵ_g	Transmittance τ_g
nit	J•(kg•K) ⁻¹	kg•m ⁻³	W•(m•K) ⁻¹	-	-
value	2230	835	1.2	0.89	0.93

3.4.3 Boussinesq approximation.

Boussinesq approximation is a conventional method to solve a non-isothermal flow as it decreases the cost of computation. This approximation is correct if the density different in values are small. In natural convection flow, we can get the fastest converge with the Boussinesq compared with the problem by setting the density of fluid as a function of temperature. Boussinesq model assumes the density of nano-fluid as a constant in all equations with the buoyancy force given as below.

$$(\rho - \rho_0) g = -\rho_0 (\beta) (T - T_0) g \dots\dots\dots 3.8$$

Boussinesq approximation neglects the temperature dependent variation in density, $\rho = \rho_0 (1 - \beta \Delta T)$, except for the buoyancy force in the momentum equation. This approximation is exact so long as various in values of density are small; precisely, the Boussinesq approximation is effective when $\beta \Delta T \ll 1$ [53].

Where:

ρ_0 is the constant density of flow, T_0 is the initial temperature, and (β) is the expansion coefficient of nano-fluid, T is temperature of nano-fluid after absorption the radiation in K.

3.4.4 Modeling Natural Convection in enclosure Domain.

When a fluid undergoes natural convection in an enclosed domain the flow field will depend on the total mass of the fluid. If this mass is not known, however the density is known, we could model the flow in one of the flowing ways:-

a- Assumption transient simulation: In this case, the density initially will be computed from the initial temperature and pressure. Consequently, the initial mass will be known. So, the mass will be conserved as the solution progress with the time. When the temperature variation in the domain is big, we should follow this approach.

- b- Assumption the steady state simulation by using the Boussinesq model (used in this study). In this approach, we will suppose the density is constant, so the mass will be specified. But, this approach is useful just when the temperature various in the nano-fluid are low, else, we should use the transient assumption.

3.4.5 Energy and momentum Equation in ANSYS FLUENT software.

Momentum equation in ANSYS FLUENT software shown in equation 3.9 below

$$\frac{\partial}{\partial t}(\rho \vec{v}) + \nabla \cdot (\rho \vec{v} \vec{v}) = -\nabla p + \nabla \cdot (\bar{\bar{\tau}}) + \rho \vec{g} \dots\dots\dots 3.9$$

Where p is the static pressure, $\bar{\bar{\tau}}$ is the stress tensor, $\rho \vec{g}$ is the gravitational body force[53].

Energy equation in ANSYS FLUENT software shown in equation 3.10 below should be done in option [54].

$$\frac{\partial}{\partial t}(\rho E) + \nabla \cdot (\vec{v}(\rho E + p)) = \nabla \cdot \left(k_{eff} \nabla T - \sum_j h_j \vec{J}_j + (\bar{\bar{\tau}}_{eff} \cdot \vec{v}) \right) + Q_{sp} \dots\dots\dots 3.10$$

Where k_{eff} is effective conductivity, The one three terms on the right-hand side expression of energy transfer because of conduction, species diffusion, and viscous dissipation, respectively, and \vec{J}_j is the diffusion flux of species j, Q_{sp} is the heat transfer between the solid surface and the other phase.

3.4.6 Radiative Transfer Equation

Radiative transfer equation 3.11 shown below in ANSYS FLUENT software for an scattering, absorbing and emitting medium at the direction (\vec{s}) in a position (\vec{r}) should be done in option when using one of radiation model. In this study discrete ordinate model(DO) is chosen ,because we have semitransparent wall (glass) and 2 different zones of fluid (water and Nano-fluid)[53].

$$\frac{dI(\vec{r}, \vec{s})}{ds} + (k_a + k_t)I(\vec{r}, \vec{s}) = K_a n^2 \frac{\sigma T^4}{\pi} + \frac{K_t}{4\pi} \int_0^{4\pi} I(\vec{r}, \vec{s}') \Phi(\vec{s}, \vec{s}') d\Omega' \dots\dots\dots 3.11$$

Where:-

\vec{r} = position vector

\vec{s} = direction vector

\vec{s}' = scattering direction vector

s = path length

k_a = absorption coefficient

n = refractive index

k_t = scattering coefficient

σ Stefan-Boltzmann constant ($5.669 \times 10^{-8} \text{ W/m}^2 \text{ K}^{-4}$)

I = radiation intensity, which depends on position and direction

T = local temperature

Φ = phase function

Ω' = solid angle

3.4.7 The Boundary Condition with Semi Transparent Wall.

In ANSYS FLUENT software we can specify exterior and interior semitransparent walls for the Discrete Ordinates model. In the case of exterior semi-transparent walls, such as glass used in this study, incident radiation will pass through the glass and transmitted to the nano-fluid. Moreover, some of radiation will refracted and transmitted to the surrounding medium, and the rest is absorbed by the nano-fluid.

Figure3.6 below shows the general case of an irradiation spectrum q_{irra} on the exterior semi-transparent wall with (0) thickness and (non-zero) absorption coefficient of the property of material.

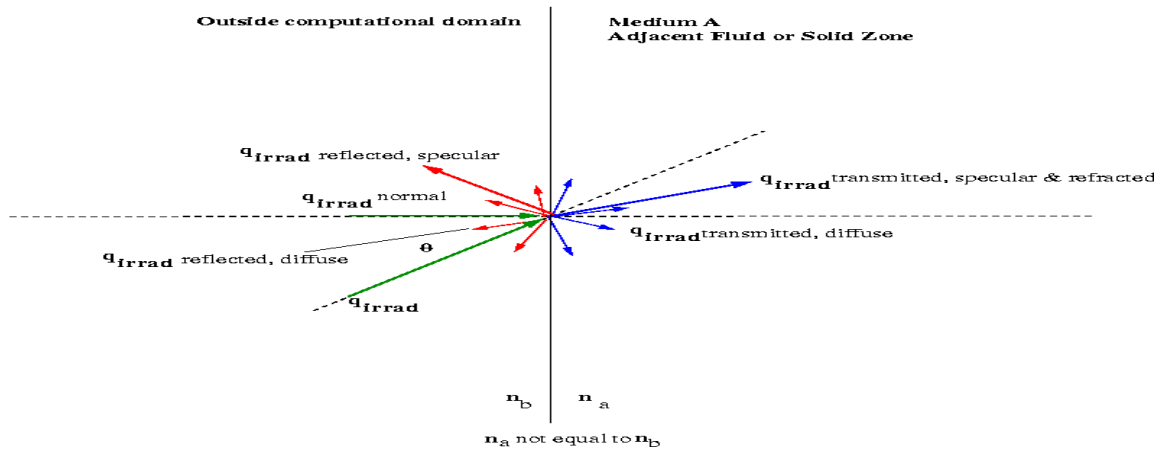


Figure 3.6:The Irradiation on External Semi-Transparent External wall[53].

3.4.8 Heat loss analysis

In order to calculate the overall heat transfer loss coefficient UL , the wind heat transfer coefficient (h_w) in natural convection is computed by equation 3.12. The heat transfer coefficient depends on the temperature of the wall surface. The values of temperature on different positions of the cells on the wall surface are different. Heat losses are due to both, radiation to the sky and convection to the ambient as shown in figure 3.7. In this study the calculation of wind heat transfer coefficient h_w is performed by assuming the wind speed V_a ranged between 2 to 5 m/s.

$$h_w = K_w * Nu / D_r \dots \dots \dots 3.12$$

Where:

Nu is the nusselt number, D_r is the diameter of glass tube 56 mm, K_w is the thermal conductivity of air .

The Reynolds number in equation 3.13 below for an air temperature that is the average of the outer tube surface and ambient temperature.

$$Re = \rho_a V_a D_r / \mu_a \dots \dots \dots 3.13$$

Where, ρ_a is the density of air = 1.25 kg/m³.

The heat transfer coefficient of wind (h_w) was found from equations 3.14, 3.15 [54] shown below

$$Nu = h_w D_r / k_w = 0.30(Re)^{0.6} \quad \text{If } (1000 < Re < 50,000) \dots\dots\dots 3.14$$

$$Nu = h_w D_r / k_w = 0.40 + 0.54(Re)^{0.52} \quad \text{If } (0.1 < Re < 1000) \dots\dots\dots 3.15$$

By substituting the wind heat transfer coefficient (h_w) in equation 3.16 shown below with a (1 m) length provides the first estimate of the loss.

$$Q_{loss} = \pi D_r L h_w (T_r - T_a) + \varepsilon_r \pi D_r L \sigma (T_r^4 - T_{sky}^4) \dots\dots\dots 3.16$$

[55].

Where:

ε_r , σ are the emissivity of glass (0.88) and Stefan-Boltzmann constant ($5.67 \times 10^{-8} \text{ W} \cdot \text{m}^{-2} \cdot \text{K}^{-4}$) respectively. (D_r) is the outer diameter of glass tube (56mm) and (T_r) is the glass wall temperature computed by ANSYS FLUENT. (K), T_{sky} is the sky temperature = $T_a - 5\text{K}$.

Q_{loss} in equation 3.16 is adopted to calculate the (UL). The loss coefficient (based on receiver area) was calculated from the equation 3.17 shown below

$$UL = \frac{Q_{loss}}{\pi D_r L (T_r - T_a)} \dots\dots\dots 3.17$$

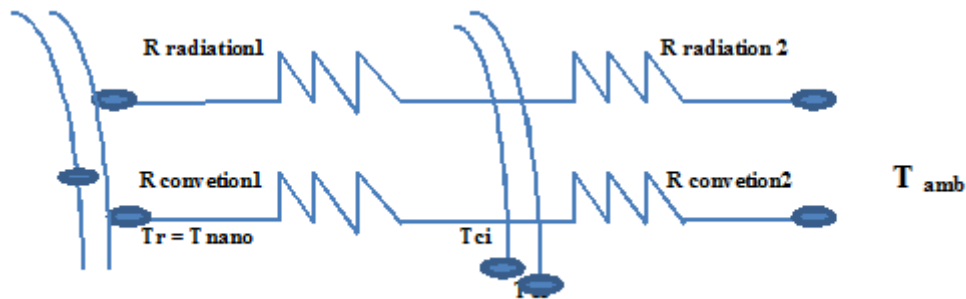


Figure 3.7: Schematic of the losses model.

3.4.9 The overall heat transfer loss coefficient (UL)UDF

In order to compute the overall heat transfer loss coefficient in equation 3.17, a User Defined Function UDF for is developed and incorporated into FLUENT. This UDF uses the position of cell center to find the surface temperature shown below.

```
#include "udf.h"

DEFINE_PROFILE(UL, thread, position)
{
    real Tsky = 295; /*skay temperature*/
    real ε = 0.88; /* emissivity of glass*/
    real ρ = 1.25; /* density of air*/
    real v = 5 ; /* velocity of air */
    real u = 0.0000179; /* viscosity of air */
    real Ka = 0.0263; /*thermal conductivity of air */
    real hw ; /*Heat transfer coefficient of air */
    real Re; /* Reynolds number of air */
    real Nu; /* nusselt number of air */
    real UL ; /* loss coefficient */
    real Dr= 0.056; /* outer diameter of receiver tube */
    real pi = 3.14;
    real L = 1; /* length of tube */
    real ε = 5.67E-08 ; /* The Stefan-Boltzmann Constant */
    real Ta = 300; /*ambient temperature of air */
    real walltemp; /* wall temperature */
    real Qloss; /*heat losses */
    cell_t c;
    real x[ND_ND]; /* this will hold the position vector */
    Re=(ρ*v*Do/u);
```

```

Nu=0.3*pow(Re,(3/5));
hw= Nu *(Ka/Do);
begin_c_loop(c,thread)
{
C_CENTROID(x, c, thread);
walltemp = C_T(c,thread) ; /* temperature of inner receiver tube */
Qloss= pi*Dr*L*hw*(walltemp-Ta)+er*pi*Dr*L*e*(pow(walltemp,4)-pow(Tsky,4));
C_PROFILE(c, thread, position) = Qloss/(pi*Dr*L*(walltemp-Ta));
}
end_c_loop(c, thread)
}

```

Where, $C_PROFILE(c, thread, position) = UL$ in equation 3.17 , $walltemp = C_T(c,thread) =$ Temperature of glass wall, $C_CENTROID(x, c, thread) =$ code to define cell center in the FLUENT (UDF).

3.5 EXPERIMENTAL INVESTIGATION

3.5.1 Introduction.

A device was built to study the heat transfer properties of the Nano-Fluid in a glass tube surrounding a copper tube for flowing the water. The main objective is to validate and the CFD simulations and the design concept. The results are taken within the range of the Reynolds number in laminar flow. The Nano-fluid used type CuOnano-particals / engine oil 5W30 with volume fraction 0.055%. The sun intensity on the surface of the receiver tube surface is measured to be $690\text{w} / \text{m}^2$ and the wind velocity is ranged between 3-5m /s.

3.5.2 General specifications of the experimental device

The experimental device consists of the following main parts: glass tube containing nano-fluid, copper tube for running water, water tank, water pump, device holder, and measuring devices. The main part of this apparatus is the heated part- the receiver unit containing copper

tube and the glass tube containing the nano-fluid. The geometry of the receiver is discussed in the following chapter.

3.5.3 Glass tube

It is a glass pipe type (Pyrex), showing its physical and thermal properties in the table (3.5) above, closed ends and filled with nano-fluid.

3.5.4 Copper tube

It is a standard copper pipe, showing its physical and thermal properties in the table (3.4) above, submerged into the nano-fluid, circulated water flowing inside it.

3.5.5 Nano-Fluid

In this experimental work, the CuO based engine oil nano-fluids was chosen and used as working fluids for the Nano-fluid Direct Absorption Solar Collector. A spherical CuO nanoparticle having the size of 200 nm and the specific surface area 80 m²/g [13] was mixed with the base fluid engine oil 5w30 by using ultrasonic mixing method to be as a suspension. The concentration of the CuO nano-particles in the base fluid was 0.055 volume ratio and the properties of the CuO nano-particles, engine oil and CuO-oil nano-fluids shown in, tables 3.2 above [13].

3.5.6 Device Holder

Both the glass tube and the copper tube are installed together on an a welded ironframe 1.05 m *1 m in dimension. This base is designed to be able to change its angles by a lever.see figure 3.8 below.

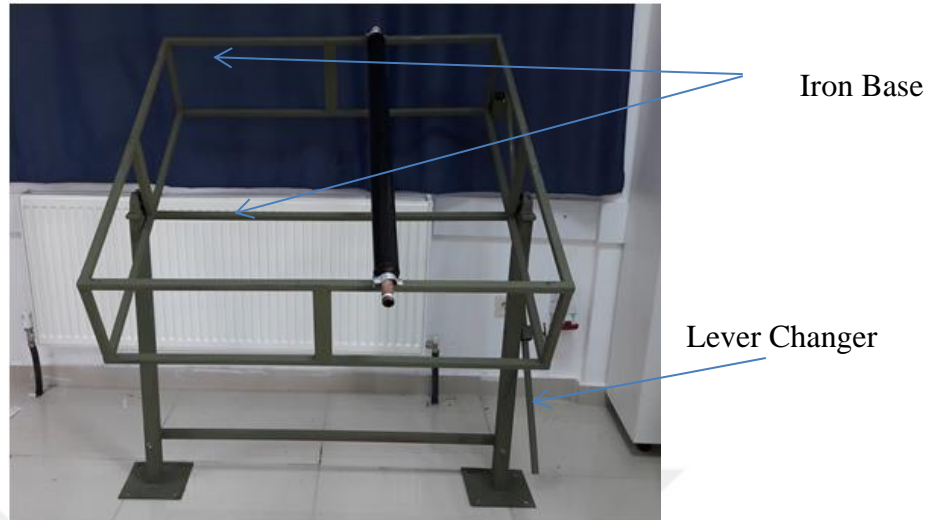


Figure 3.8: Device Holder

3.5.7 The measurement system

The measurement system consists of water temperature measuring devices of the two inlet and outlet sections, the ambient temperature mete, the solar radiation intensity meter and water flow meter. The necessary calibration has been performed for the devices that need it.

3.5.7.1 Water Flow Meter

The flow meter type LZS-15 with the capacity of volume flow rate (3-100 L / H) shown in figure 3.9 below was used to measure the flow rate of the water that entering the copper pipe.

The outlet section of the flow meter was connected to the inlet section of the copper tube by a rubber tube and the inlet section was connected to the water tank. The amount of water entering the copper tube can be controlled by using a check valve figure 3.10 putted it before the inlet of flow meter and thus the control of Reynolds number in laminar.



Figure 3. 9: Water flow meter.



Figure 3.10: Check valve.

3.5.7.2 Temperature measuring system (Thermocouples).

The temperatures were measured except the ambient temperature by using a tow thermocouples type (K) (0.2mm) in diameter Figure 3.11below. These were installed one on the copper tube inlet and the other on the outlet to measure the temperature of the water inlet and outlet.

Thermocouples were calibrated prior by using the boiling water to calibrate the thermocouples. The thermocouples were installed in the boiling water and the other end was connected by Arduinio Type (SAPPA-103) Figure 3.12 below to the computer after installation the application of it to read the results and compare them with the results of thermostat in the same boiling water where it was found that the difference between them ranges from (0.5 – C°)



Figure 3. 11: Thermocouples type (K 0.2mm)

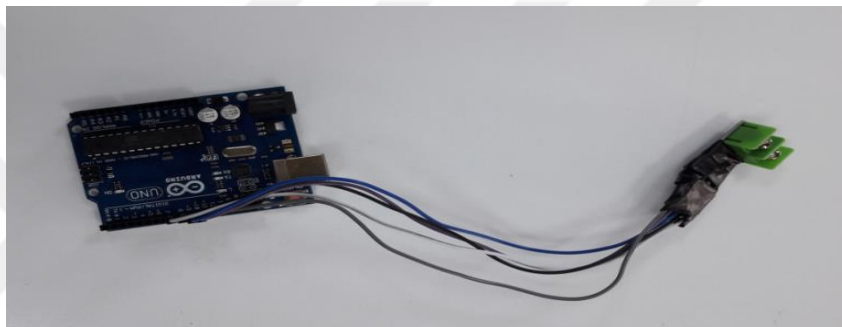


Figure 3. 12: Arduino Type (SAPPA-103)

3.5.7.3 Solar radiation intensity meter.

The solar irradiance intensity was measured by using (Okapi Solar Calculator Application) shown in Figure 3.13 below. The application installed on android smart phone, and calibrated by using a lamp Type (500 Lumens and 8 watts) and filter putted it on the light sensor of the phone.

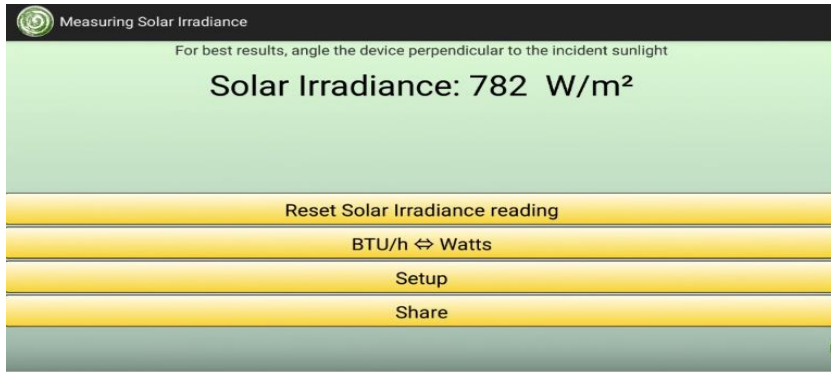


Figure 3. 13: Interface of measuring solar irradiance application.

CHAPTER FOUR

RESULTS AND DISCUSSIONS

4.1 Introduction

In this chapter, the results of this study are divided into two parts. Firstly, the CFD results, obtained from the numerical solution for three models by using the simulation in ANSYS FLUENT software with steady state case for choosing the optimum design is performed. Secondly, an experimental apparatus, corresponding to the highest performance configuration identified by the CFD study is constructed and measurement obtained.

4.2 Heat convective of three models calculation.

To compare the steady state operating characteristics of the NDASC for three models with size ratio of 1/4, 1/2, and 3/4, it was assumed that the following operational parameters remained unchanged with time; the global solar radiation intensity at 877 W/m^2 , ambient air temperature at 300K, and inlet mass flow rate of water inside the copper tube is 0.001 kg/s . To find the best collector model, one should calculate the convection heat transfer per unit length across the nano-fluid space between tubes for all models. This is performed below by calculating the effective thermal conductivity of nano-fluid k_{eff} , Kinematic viscosity ν , Thermal diffusivity α , Length scale used in the Rayleigh number L_c , Rayleigh Number Ra and Prandtl number Pr of nano-fluid for all model. T_n is the maximum nano-fluid temperature obtained from ANSYS FLUENT, r_i , r_o are the radius of copper tube and glass tube respectively for each of the models [39].

4.2.1 Heat convective in model with glass /copper tube diameter ratio (1/4).

ANSYS FLUENT simulation is used to obtain the temperature of nano-fluid, T_n (see figure4.1).The computed heat transfer, for model $\frac{1}{4}$ ratio calculated as shown below.

$$L_c = \frac{2[\ln(\frac{r_o}{r_i})]^{4/3}}{(r_i^{-3/5} + r_o^{-3/5})^{5/3}}$$

$$L_c = \frac{2[\ln(0.0255/0.006375)]^{4/3}}{(0.006375^{-3/5} + 0.0255^{-3/5})^{5/3}} = 0.0108 \text{ m}$$

$$Ra = \frac{g\beta(T_n - T_a)L_c^3}{\nu\alpha}$$

$$Ra = \frac{9.81 * 0.0006996(326 - 300) * 0.0108^3}{8.7 * 10^{-8} * 7.48 * 10^{-5}} = 34541.6$$

$$Pr = \nu/\alpha$$

$$Pr = \frac{(7.48 * 10^{-5})}{(8.7 * 10^{-8})} = 860$$

$$K_{eff} = 0.386K \left(\frac{Pr}{0.861 + Pr} \right)^{1/4} (Ra_c)^{1/4} = 0.712 (W m^{-1} k^{-1})$$

$$K_{eff} = 0.3386 * 0.14 \left(\frac{860}{0.861 + 860} \right)^{1/4} (34541.6)^{1/4} = 0.73 (W m^{-1} k^{-1})$$

$$q' = \frac{2\pi K_{eff}}{\ln(\frac{r_o}{r_i})} (T_n - T_a)$$

$$q' = \frac{2 \cdot 3.14 \cdot 0.73}{\ln(0.0255/0.006375)} (326-300) = 86 \text{ W/m}$$

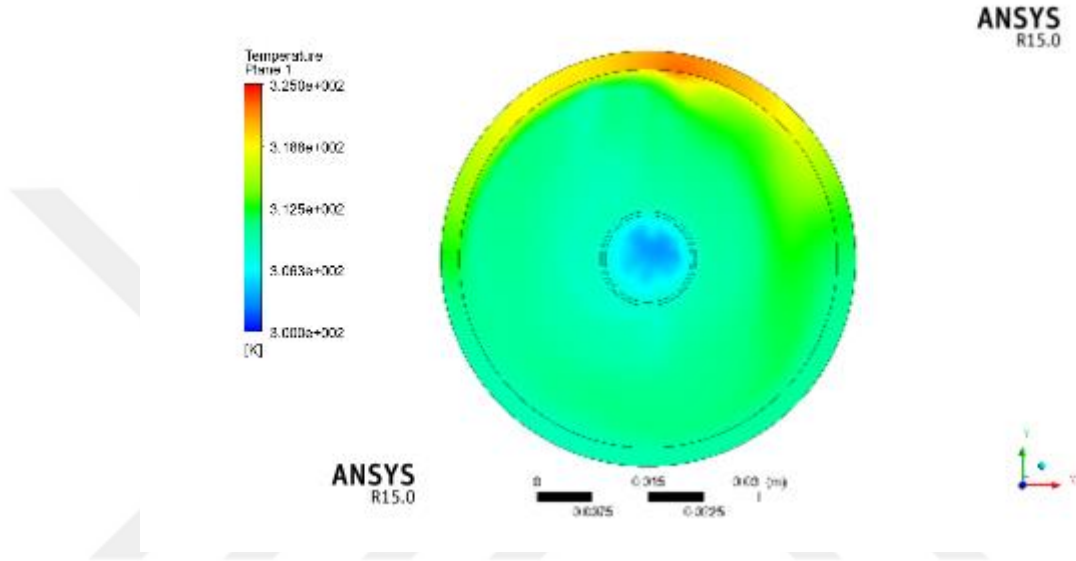


Figure 4. 1: Temperature distribution, simulated by ANSYS at $z = 0.95 \text{ m}$ in the model (1/4).

4.2.2 Heat convective model with glass/copper tube diameter ratio (1/2).

ANSYS FLUENT simulation is used to obtain the temperature of nano-fluid, T_n (see figure 4.2). The computed heat transfer, for model 1/2 ratio calculated as shown below.

$$L_c = \frac{2[\ln(r_o/r_i)]^{4/3}}{(r_i^{-3/5} + r_o^{-3/5})^{5/3}}$$

$$L_c = \frac{2[\ln(0.0255/0.0125)]^{4/3}}{(0.0125^{-3/5} + 0.0255^{-3/5})^{5/3}} = 6.9 \times 10^{-3} \text{ m}$$

$$Ra = \frac{g\beta(T_n - T_a)L_c^3}{\nu\alpha}$$

$$Ra = \frac{9.81 * 0.0006996 (322 - 300) * 0.0069^3}{8.7 * 10^{-8} * 7.48 * 10^{-5}} = 7622$$

$$Pr = \nu / \alpha$$

$$Pr = \frac{(7.48 * 10^{-5})}{(8.7 * 10^{-8})} = 860$$

$$K_{eff} = 0.386k \left(\frac{Pr}{0.861 + Pr} \right)^{1/4} (Ra_c)^{1/4}$$

$$K_{eff} = 0.386 * 0.14 \left(\frac{860}{0.861 + 860} \right)^{1/4} (12089)^{1/4} = 0.506 \text{ (W m}^{-1} \text{ k}^{-1}\text{)}$$

$$q' = \frac{(2\pi K_{eff})}{\ln(r_o/r_i)} (T_n - T_a)$$

$$q' = \frac{(2 * 3.14 * 0.506)}{\ln(0.0255/0.0125)} (322 - 300) = 98.04 \text{ W/m}$$

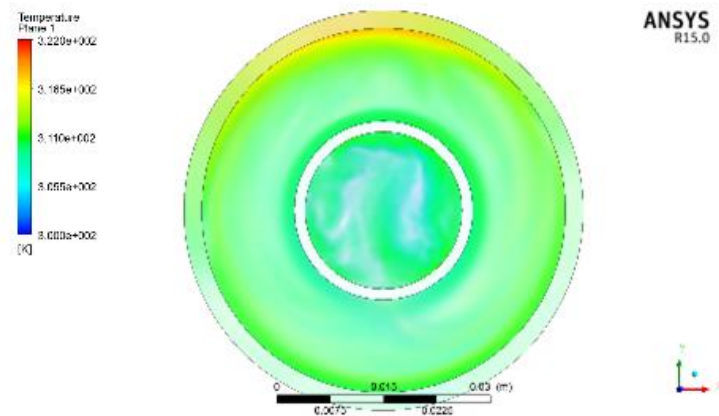


Figure 4.2: Temperature distribution, simulated by ANSYS at $z = 0.95$ m in the model (1/2).

4.2.3 Heat convective model with glass /copper tube diameter ratio (3/4).

ANSYS FLUENT simulation is used to obtain the temperature of nano-fluid, T_n (see figure4.3).The computed heat transfer, for model 3/4 ratio calculated as shown below.

$$L_c = \frac{2[\ln(r_o/r_i)]^{4/3}}{(r_i^{-3/5} + r_o^{-3/5})^{5/3}}$$

$$L_c = \frac{2[\ln(0.0255/0.019125)]^{4/3}}{(0.019125^{-3/5} + 0.0255^{-3/5})^{5/3}} = 2.687 \times 10^{-3} \text{ m}$$

$$Ra = \frac{g\beta(T_n - T_a)L_c^3}{\nu\alpha}$$

$$Ra = \frac{9.81 * 0.0006996(315 - 300) * 0.002687^3}{8.7 * 10^{-8} * 7.48 * 10^{-5}} = 306$$

$$Pr = \nu/\alpha$$

$$Pr = \frac{(7.48 * 10^{-5})}{(8.7 * 10^{-8})} = 860$$

$$K_{eff} = 0.386k \left(\frac{Pr}{0.861 + Pr} \right)^{1/4} (Ra_c)^{1/4}$$

$$K_{eff} = 0.386 * 0.14 \left(\frac{860}{0.861 + 860} \right)^{1/4} (306)^{1/4} = 0.225 \text{ (W m}^{-1} \text{ k}^{-1}\text{)}$$

$$q' = \frac{(2\pi K_{eff})}{\ln(r_o/r_i)} (T_n - T_a)$$

$$q' = \frac{2 * 3.14 * 0.225}{\ln(0.0255/0.019125)} (315 - 300) = 73.6 \text{ w/m}$$

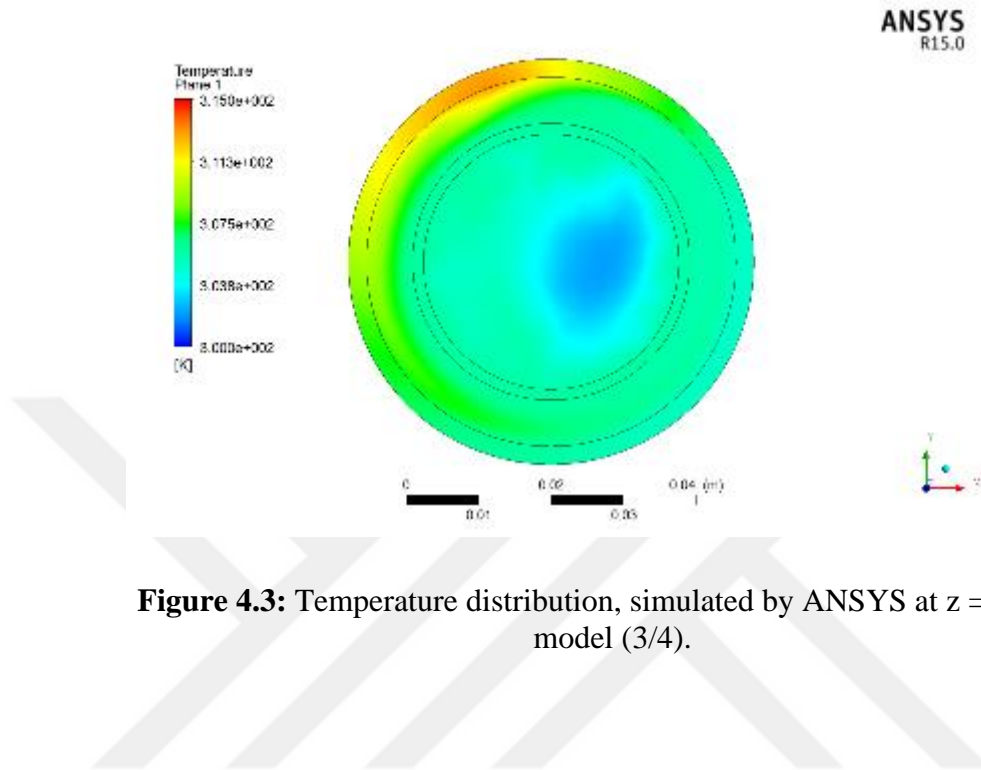


Figure 4.3: Temperature distribution, simulated by ANSYS at $z = 0.95$ m in the model (3/4).

Where:

$$\alpha \text{ is the thermal diffusivity} = \frac{k}{\rho \cdot C_p}$$

$$\nu \text{ is the kinematic viscosity} = \frac{\mu}{\rho}$$

4.3 Velocity stream line between nano-fluid and copper tube.

Thermal and dynamic behavior of nano-fluid inside three models of solar collector for the NDASC were numerically calculated and compared. Figures 4.4, 4.5 and 4.6 shows the streamlines in the plan at $z = 0.95$ m and the vortices due to natural convection at 300 K inlet temperature, solar radiation intensity 877 W/m² and mass flow rate of water 0.001kg/s for each model. For the model with the ratio of 1/4 vortex movement of nano-fluid upward and downward is observed, the velocity of streamline near the copper tube wall rises slightly more than the glass tube wall. The figure 4.5 which shows the model with the ratio of 1/2, the velocity of streamline near copper tube wall is much more than velocity near glass wall, as the

velocity of the streamline was higher near the copper pipe wall compared to the wall of the glass tube that means the heat exchange between nano-fluid and copper tube walls is higher than the heat exchange between nano-fluid and glass tube walls, which in turn reduces the heat losses due to lack thermal exchange between nano-fluid and glass wall, this causes to increase the performers and efficiency of the solar collector. For the model 3/4 was the lowest streamline velocity between the three models as shown in figure 4.6 and the amount of nano-fluid was the least compared with two models. This led to the heat lowest heat transfer to the copper wall from the nano-fluid.

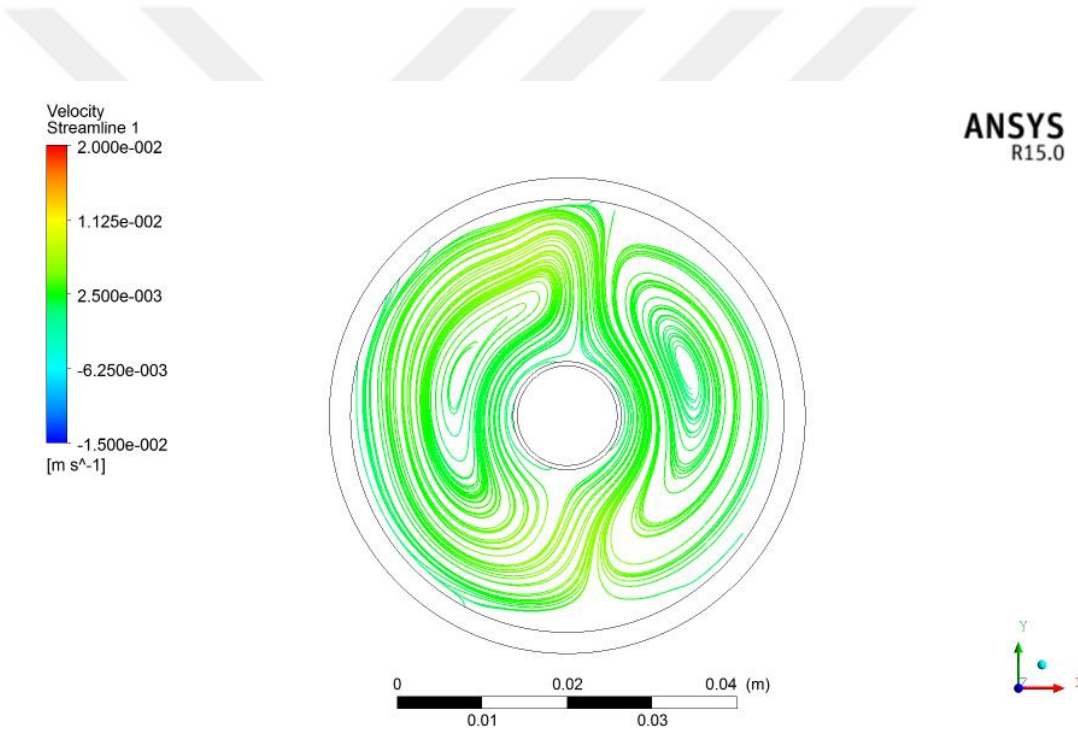


Figure 4.4: Streamlines in the plan at $z = 0.75$ m showing the vortices due to natural convection model (1/4). At 300 k inlet temperature and 0.001kg/s.

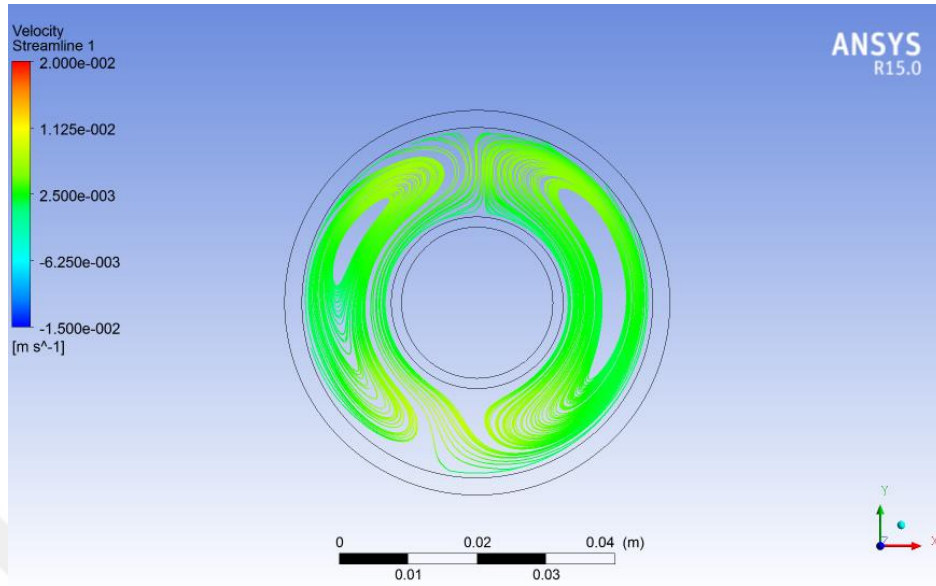


Figure 4.5: Streamlines in the plan at $z = 0.75$ m showing the vortices due to natural convection model (1/2). At 300 k inlet Temperature and 0.001kg/s.

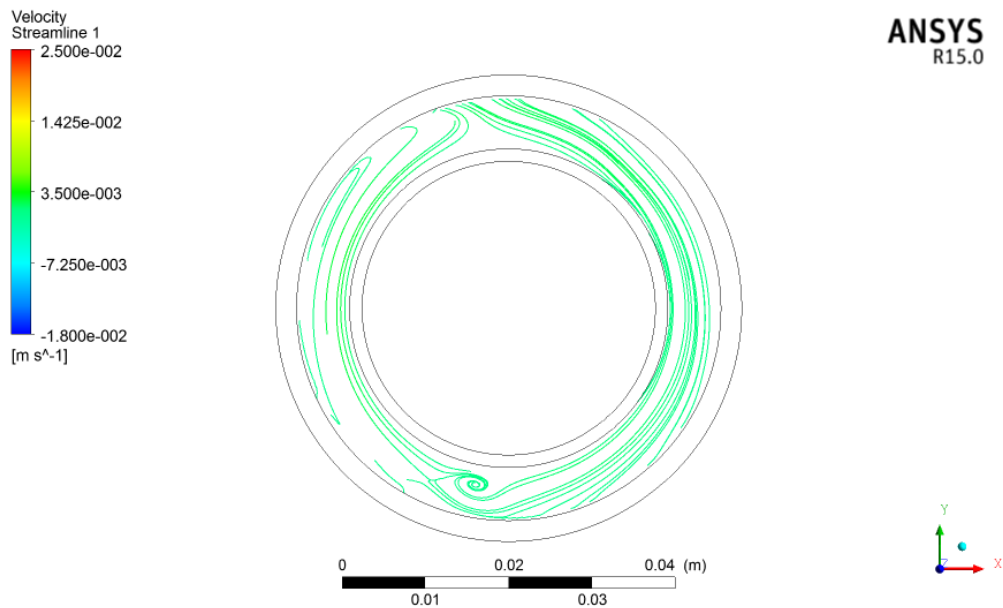


Figure 4.6: Streamlines in the plan at $z = 0.75$ m showing the vortices due to natural convection model (3/4). At 300 k inlet Temperature and 0.001kg/s.

4.4 Efficiency of models with different value of water mass flow rate.

The figure 4.7 shows, for each model, the efficiency of absorption in thermal efficiency when increased the mass flow rate of water. The efficiency is increase due to the increased value of Reynolds' number but still in laminar flow region in this research. This led to decrease the outlet temperature as shown below in tables 4.1, 4.2, 4.3. The above observations is consentient the theoretical results and equation of thermal efficiency:

$$\eta = \frac{\dot{m} C_p \Delta T}{A_s I} * 100\%$$

Where:-

ΔT is different between inlet and outlet temperature of water in K as shown in figures 4.8, 4.9, 4.10 below, I is the sun radiation intensity W/m^2 , A_s is the surface area of glass tube.

Figure 4.9 shows the graduate, downstream increase of water temperature as it flows along the copper tube.

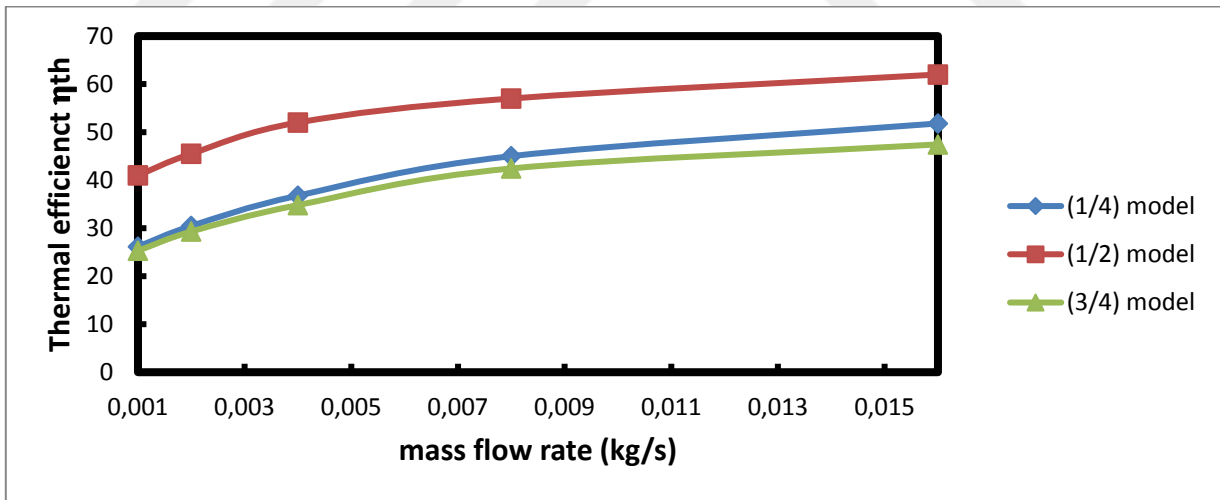


Figure 4.7: Efficiency with different mass flow rate of water for three models (1/4),(1/2),(3/4) obtained from ANSYS program simulation.

Table4.1: Theoretical results of model ¼ obtained from ANSYS program simulation.

Water mass flow rate kg/s	Water Inlet temperature K	Water outlet temperature K	ΔT K	η %
0.001	300	309.62	9.62	26.16
0.002	300	305.6	5.6	30.46
0.004	300	303.38	3.38	36.77
0.008	300	302.07	2.07	45
0.016	300	301.19	1.19	51.8

Table4.2: Theoretical results of model ½ obtained from ANSYS program simulation.

Mass flow rate kg/s	Inlet Tempe K	Outlet Tempe K	ΔT K	η %
0.001	300	315.11	15.11	41
0.002	300	308.57	8.57	46.4
0.004	300	304.8	4.8	52
0.008	300	302.6	2.6	56.4
0.016	300	301.428	1.428	61.9

Table4.3: Theoretical results of model ¾ obtained from ANSYS program simulation.

Mass flow rate kg/s	Inlet Tempe K	Outlet Tempe K	ΔT K	η %
0.001	300	309.3	9.3	25.3
0.002	300	305.4	5.4	29.3
0.004	300	303.2	3.2	34.7
0.008	300	301.95	1.95	42.32
0.016	300	301.09	1.09	47.236

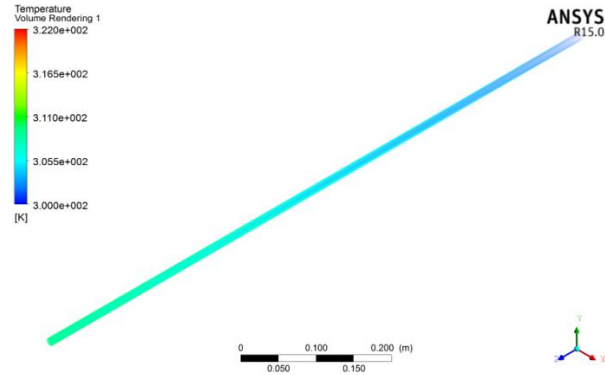


Figure 4.8: Temperature distribution in interior water for model 1/4 with mass flow rate 0.001kg/s .

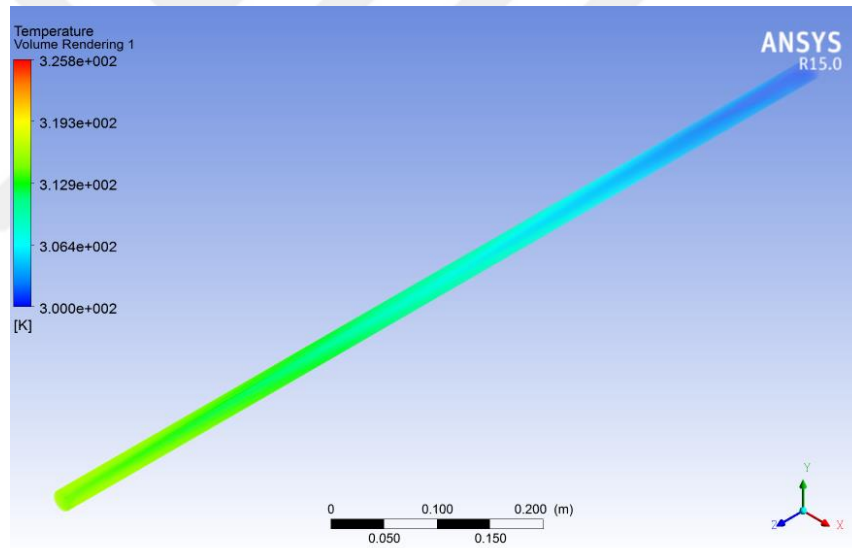


Figure 4.9: Temperature distribution in interior water for model 1/2 with mass flow rate 0.001kg/s.

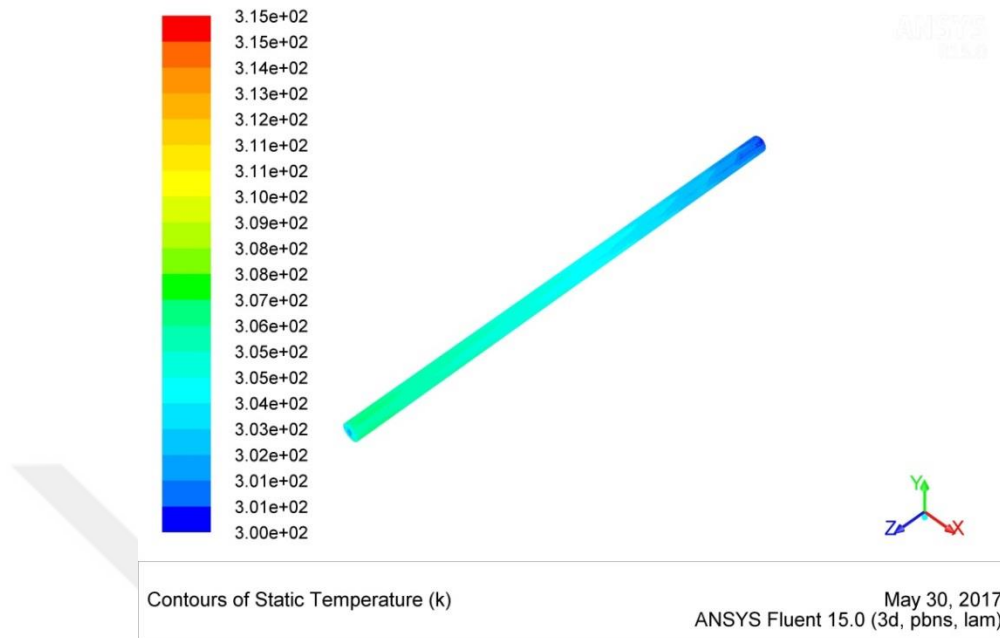


Figure 4.10: Temperature distribution in interior water for model 3/4 with mass flow rate 0.001kg/s.

4.5 Chosen of optimum model

From sections 4.2, 4.3, 4.4 we find that the simulated efficiency of 1 metersolar receiver with glass-to-copper tube size ratios of 1/4, 1/2, and 3/4 to be 51.8%, 61%, and 47%, respectively. Above efficiencies are obtained for mass flow rate of 0.016 kg/s. Circulating water restricts the raising of nano-fluid temperature and in turn reduces thermal losses. Inside the copper tube, water flow rate changes increasingly affect the efficiency for all size ratios. In nano-fluid region, both of depth of absorption in nano-fluid and characteristic length of natural convection significantly affects the receiver unit efficiency. In size ratio of 3/4, the insufficient depth of absorption was behind the efficiency shortness. While in size ratio of 1/4, the insufficient area of convection was behind the efficiency shortness. The optimum size ratio, which results in sufficient absorption depth and sufficient convection area, is the size ratio of 1/2.

4.6 Experimental results

The optimum model, of ratio 1/2, obtained from ANSYS simulation is manufactured to perform the experiments. The measured values are compared to simulation values. Five experiments with mass flow rates ranging from 0.001kg/s to 0.016 kg/s is performed. The solar radiation intensity is 690 W/m² and ambient temperature is 300K. The experimental results was compared with theoretical results by using simulation in ANSYA program to calculate the error percent as shown in table 4.4 below.

Table4.4: The comparison of Numerical and Experimental of model ½ with inlet water temperature 300k.

	CFD results	Experimental results	
Mass flow rate of water (kg/s)	ΔT (k) of water	ΔT (k) of water	Error%
0.001	10.2	9.78	4.117
0.002	5.65	5.38	4.77
0.004	3.15	3.020	4.12
0.008	1.7	1.63	4.05
0.016	1	0.961	3.82

$$\text{Where: Error \%} = 1 - \frac{\text{Experimental } \Delta T}{\text{Numerical } \Delta T} * 100\%$$

From table 4.4 we find that the error percentage ranged from 3.82 to 4.77 % with different mass flow rates of water. Figure 4.11 and tables 4.5, 4.6 below shows the change in efficiency of collector with different mass flow rate of water in numerical and experimental results respectively.

Table4.5: Numerical Results of model 1/2.

Mass flow rate kg/s	Inlet Tempe K	Outlet Tempe K	ΔT K	η %
0.001	300	310.2	10.2	35.15
0.002	300	305.65	5.65	39
0.004	300	303.15	3.15	43.4
0.008	300	301.7	1.7	46.8
0.016	300	301	1.00	55.16

Table4.6: Experimental Results of model 1/2.

Mass flow rate kg/s	Inlet Tempe K	Outlet Tempe K	ΔT K	η %
0.001	300	309.78	9.78	33.7
0.002	300	305.38	5.38	37.07
0.004	300	303.020	3.020	41.62
0.008	300	301.63	1.63	45
0.016	300	300.961	0.961	53.0

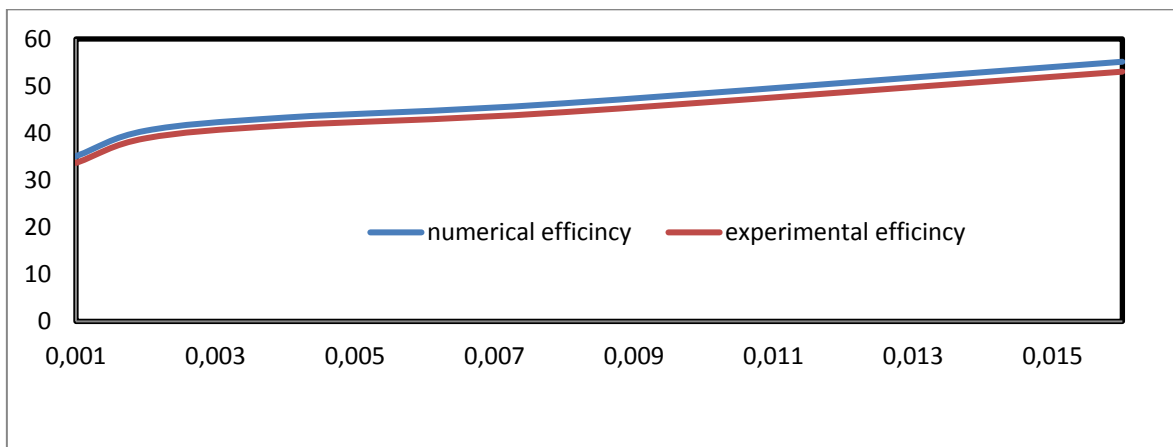


Figure 4.11: The comparison of theoretical and experimental Efficiency with different mass flow rate of water for model 1/2.

4.7 Effect of inlet water temperature on the efficiency.

The figure 4.12 shows the efficiency of the solar collector as the mass flow rate increases. As the inlet water temperature is increased the efficiency is reduced. The solar radiation intensity is constant.

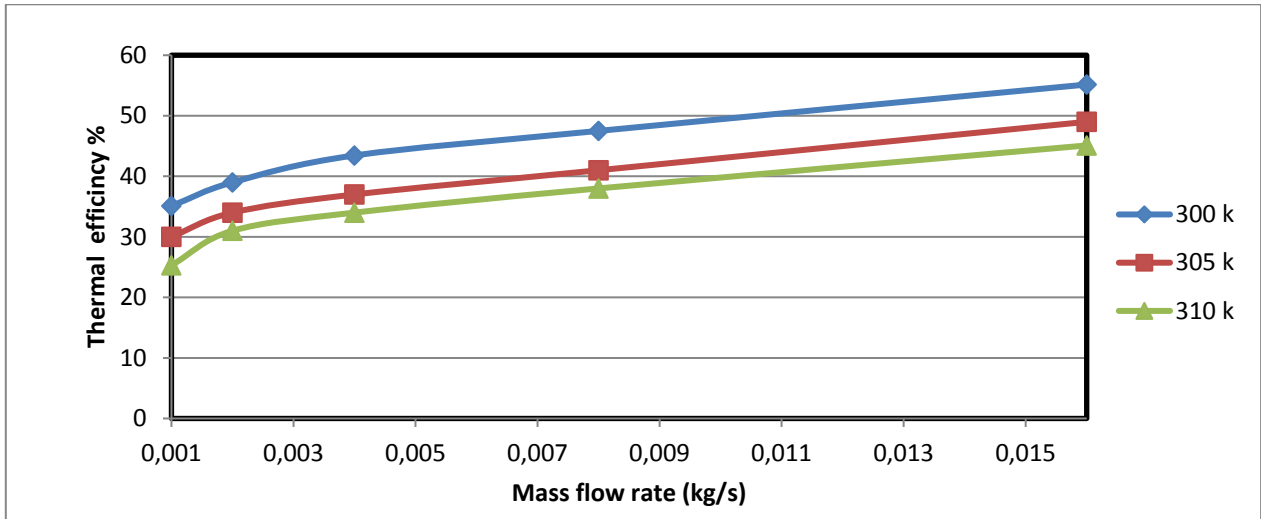


Figure 4.12: Thermal efficiency change with temperature inlet fluid.

Table4.7: Experimentally effect of different inlet temperature on the outlet temperature and thermal efficiency ratio ½ models.

	300 k	Efficiency%	305 k	Efficiency%	310 k	Efficiency%
Mass flow rate (kg/s)	ΔT (k)		ΔT (k)		ΔT (k)	
0.001	9.78	33.7	8.7	30	7.33	25.3
0.002	5.38	37.07	5.0	34.46	4.49	31
0.004	3.02	41.61	2.67	37	2.46	34
0.008	1.63	45	1.48	41	1.377	38
0.016	0.961	53	0.89	49	0.817	45.1

Table 4.7 shows the efficiency and the outlet temperature for the different mass flow rates. As the inlet water temperature is increased the thermal gradient between nano-fluid and water is decreased resulting in reduced heat flux. The downstream increase the water temperature also causes reduction in heat flux. The downstream increase in the temperature is also evident along the outer glass surface of model see figure 4.14.

4.8 Temperatures distribution in the model (1/2)

CFD simulations show that the temperature distribution of the glass wall on Figure 4.13. Different values of temperature in glass wall region are observed because of the different in the rate of exchange of heat with the water along the tube.

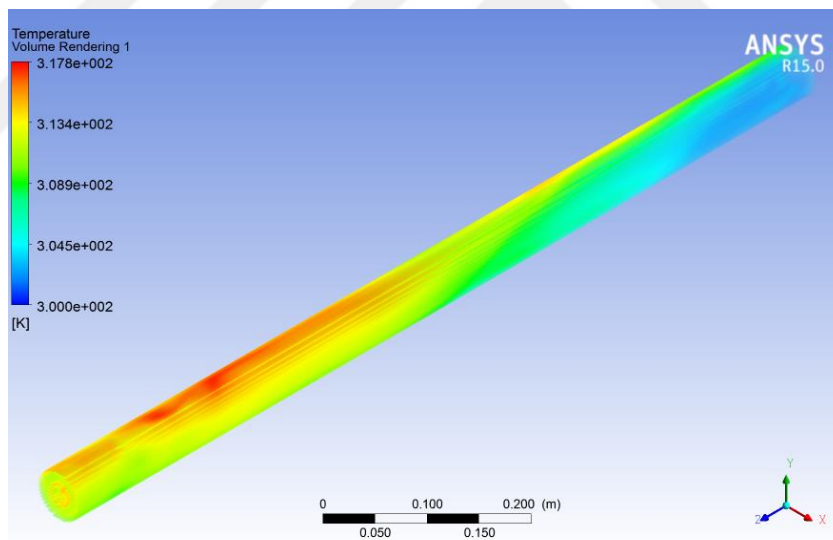


Figure 4.13: Temperature distribution along the glass wall of the ratio $\frac{1}{2}$ model.

4.9 Temperatures distribution of the water.

We can see the temperature distribution in interior water region on the model in figure 4.14 below, showing an increase in temperature with the direction of flow.

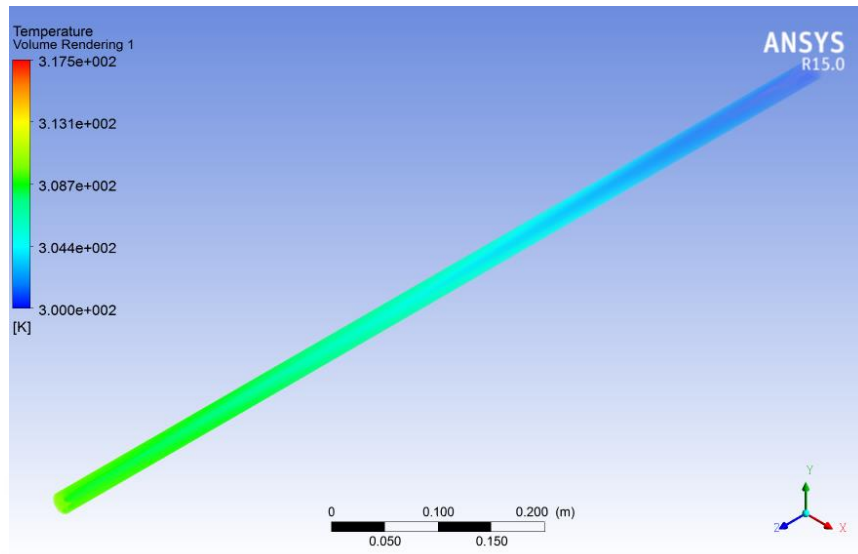


Figure 4.14: The interface temperature distribution between the inside of copper tube and the flowing water of the ratio $\frac{1}{2}$ models

4.10 Velocity streamline in nano-fluid.

The temperature differences between the external glass tube and the internal copper tube, coupled with the gravitational field, create buoyancy driven spiraling flow bottom within the Nano-fluid region. See figure 4.15 below.

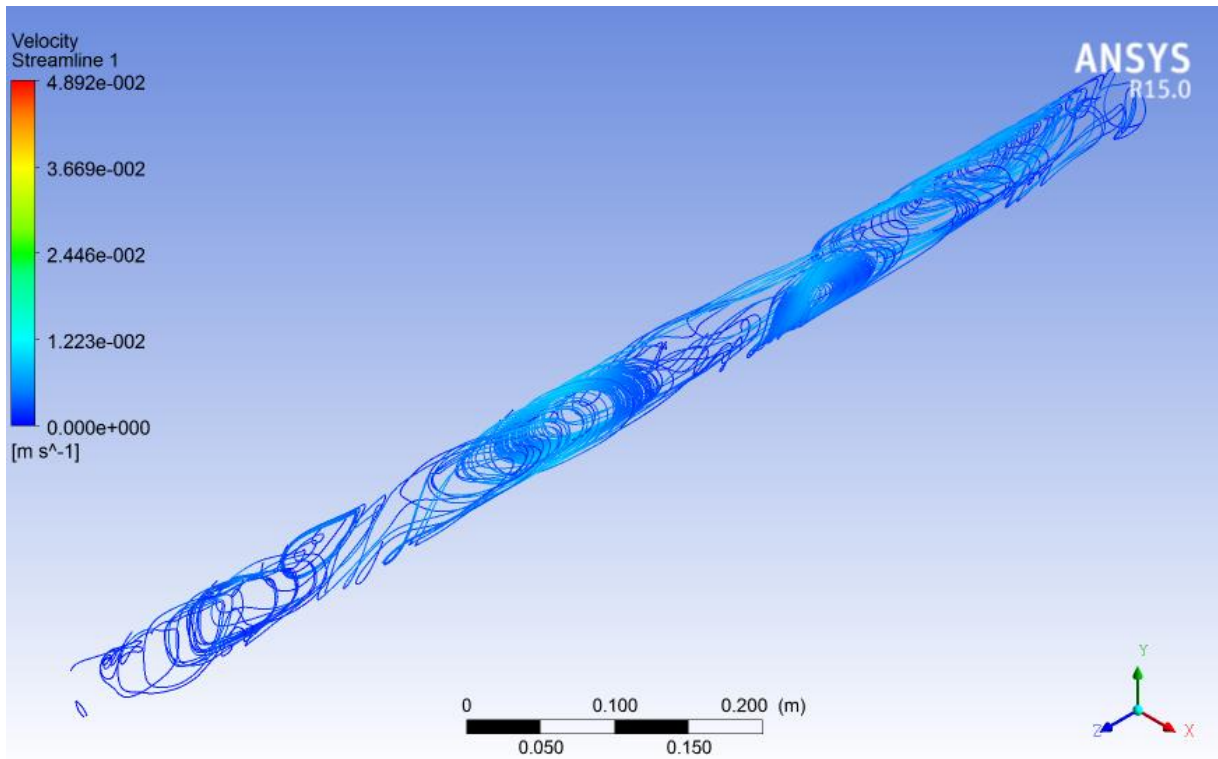


Figure 4.15: Velocity streamline in nano-fluid of the ratio $\frac{1}{2}$ model.

4.11 Changing in the distribution of nano-fluid temperature with different inlet water temperature and different mass flow rate.

We can see when increasing the mass flow rate of water from 0.001kg/s to 0.002 kg/s with constant inlet water temperature at 300K lead to increase the heat exchange between the Nano-fluid and the water flowing in the copper tube along the collector. So this increase in the heat exchange lead to a heat distribution in the nano-fluid more regular, see figures 4.16,4.17 below.

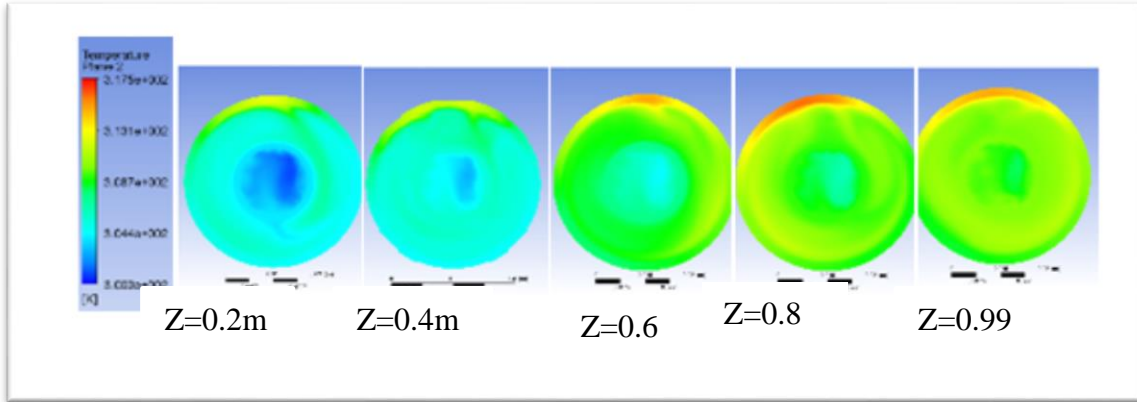


Figure 4.16: Temperature distributions at different value of Z direction with 300K inlet temperature and 0.001 kg/s mass flow rate of water for the ratio $\frac{1}{2}$ model.

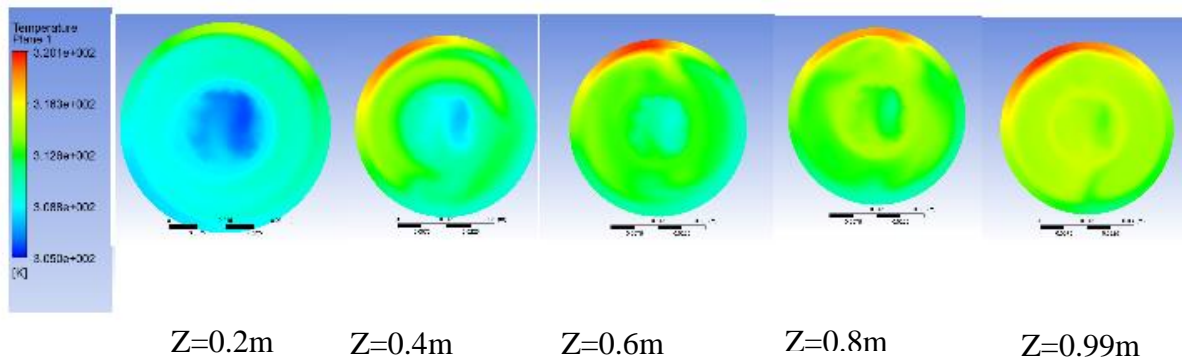


Figure 4.17: Temperature distributions at different value of Z direction 300K inlet temperature and 0.002 kg/s mass flow rate of water for the ratio $\frac{1}{2}$ model.

We can see from figures 4.18, 4.19 below with same mass flow rates of water above, but with inlet water temperature at 305K lead to decrease the heat convection from the nano-fluid to the water.

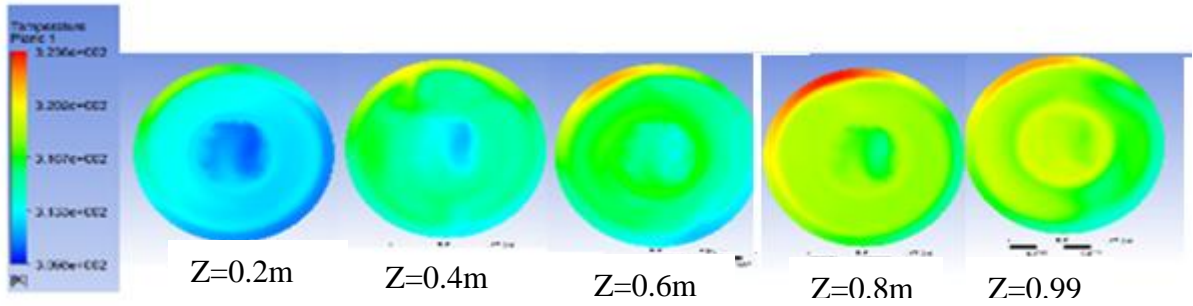


Figure 4.18: Temperature distributions at different value of Z direction 305K inlet temperature and 0.001 kg/s mass flow rate of the ratio $\frac{1}{2}$ model.

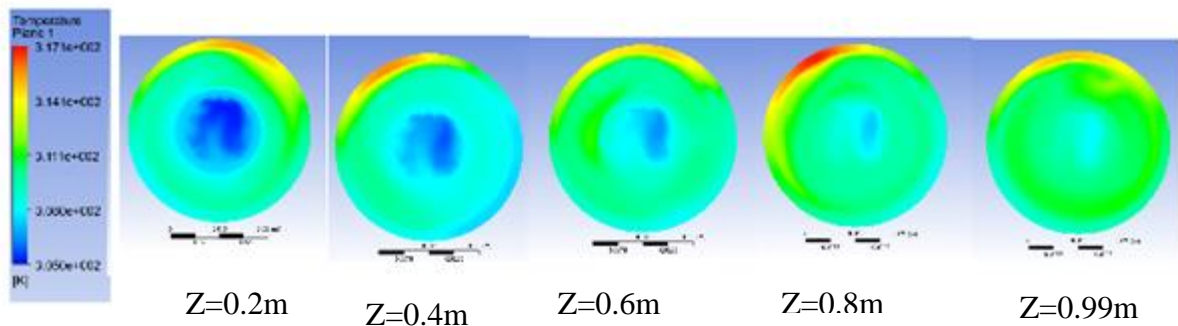


Figure 4.19: Temperature distributions at different value of Z direction 305K inlet temperature and 0.002 kg/s mass flow rate of the ratio $\frac{1}{2}$ model.

Figures 4.20, 4.21 below shows more decrease in heat convection with same mass flow rates of water but with inlet temperature at 310 K.

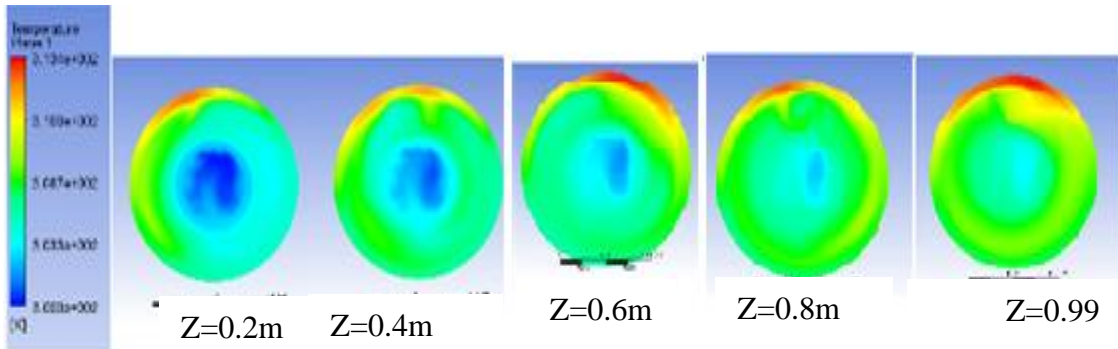


Figure 4.20: Temperature distributions at different value of Z direction 310K inlet temperature and 0.001 kg/s mass flow rate of the ratio $\frac{1}{2}$ model.

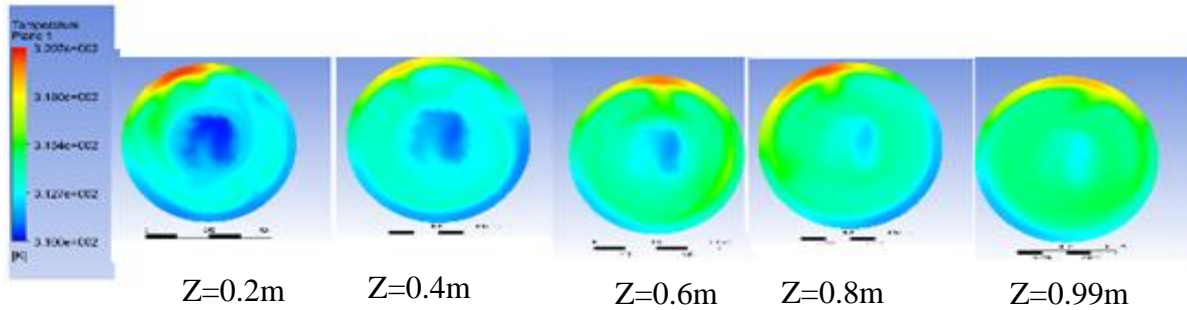


Figure 4.21: Temperature distributions at different value of Z direction 310K inlet temperature and 0.002 kg/s mass flow rate of the ratio $\frac{1}{2}$ model.

4.11 Cost of the model.

After comparison between the cost of manufacturing of the study model for 1 tubes in solar collector with a conventional solar collector that used indirect heat exchanger we found that the cost of the study model was 340\$, and the cost of the conventional model of solar collector about 800\$ because the conventional model needs to a high amount of nano-fluid for circulating it in along pipe leads to increase the thermal resistance.

CHAPTER FIVE

CONCLUSIONS AND FUTURE WORK

5.1 Conclusion

Novel direct absorption solar collectors (DASC) using copper oxide nanoparticle-based nano-fluid as a working fluid have been investigated theoretically as a function of the size ratio between the receiver tube and the copper tube for three models, and experimentally for the optimum model. The measured optical properties of the nano-fluid has been considered and used in the fluid dynamics simulations, taking into account both the optical ray-tracing and 3D heat transfer analysis. The single tube collector operating with a (none circulating) nano-fluid in the presence of convection heat losses has been modeled. A none-circulating nano-fluid absorbs solar radiation through glass wall. The absorbed heat directly transfers to circulated water flowing inside the copper tube submerged in the nano-fluid. The efficiency of a solar collector depends on the nano-fluid amount, the area of heat exchanging between the water and nano-fluid and on the mass flow rate of water.

Inclined receiver tube was studied numerically by using FLUENT ANSYS software for three models which consists of flowing water, nano-fluid annular region and the copper tube which separates the two different fluids. The efficiency of 1 meter long collector with glass-to-copper tube diameter ratios of 1/4, 1/2, and 3/4 is studied. The simulated efficiencies, compared to the evacuated tube collector, were respectively; 51.8%, 61%, and 47%. The sun radiation intensity is 877 W/m².

The circulating water in the copper tube restricts the raising of nano-fluid temperature and in turn reduces thermal losses. Increasing the flow rate of the water, reduces the temperature difference between the nano fluid and the water, leads to increased efficiency. In nano-fluid region, both the depth of absorption in nano-fluid and characteristic length of natural convection significantly affects the receiver unit efficiency.

In size ratio of 3/4, the insufficient depth of absorption was behind the observed low efficiency, while in size ratio of 1/4, the insufficient cross-sectional area of convection was behind the efficiency shortness. The optimum size ratio, which results in sufficient absorption

depth and sufficient convection area, appears in the size ratio of 1/2. Optimum model was tested experimentally and theoretically with sun radiation intensity 690 w/m². The error percentage between Experimental and theoretical results were limited between 3.82% and 4.1 %.

5.2 Future Works

The results of this research are very interesting and encouraging us to adopt and further develop this project. Moreover, the most important suggestion for future work is to test more models with use of different type of base fluids, different type and size of nanoparticles, and different value of concentration of nanoparticle in the base fluid both theoretically and experimentally. The above variables can be investigated to obtain the optimal collector for a given solar intensity. One could also use evacuated tube to cover the receiver tube to decrease the heat losses in the experimental part.

REFERENCESE

1. Xia, X. and J. Xia. *Evaluation of potential for developing renewable sources of energy to facilitate development in developing countries*. in *Power and Energy Engineering Conference (APPEEC), 2010 Asia-Pacific*. 2010. IEEE.
2. Verma, S.K. and A.K. Tiwari, *Progress of nanofluid application in solar collectors: a review*. *Energy Conversion and Management*, 2015. **100**: p. 324-346.
3. Suman, S., M.K. Khan, and M. Pathak, *Performance enhancement of solar collectors—A review*. *Renewable and Sustainable Energy Reviews*, 2015. **49**: p. 192-210.
4. Javadi, F., R. Saidur, and M. Kamalisarvestani, *Investigating performance improvement of solar collectors by using nanofluids*. *Renewable and Sustainable Energy Reviews*, 2013. **28**: p. 232-245.
5. Hussein, A., A. Walunj, and L. Kolsi, *Applications of nanotechnology to enhance the performance of the direct absorption solar collectors*. *Journal of Thermal Engineering*, 2016. **2**: p. 529-540.
6. Allamraju, K., *Materials used for renewable energy resources*. *Advanced Materials Manufacturing and Characterization*, 2013. **3**: p. 243-248.
7. Hussein, A.K., *Applications of nanotechnology in renewable energies—A comprehensive overview and understanding*. *Renewable and Sustainable Energy Reviews*, 2015. **42**: p. 460-476.
8. Parida, B., S. Iniyar, and R. Goic, *A review of solar photovoltaic technologies*. *Renewable and sustainable energy reviews*, 2011. **15**(3): p. 1625-1636.
9. Fuentes, R.G., et al., *Study of thermal diffusivity of nanofluids with bimetallic nanoparticles with Au (core)/Ag (shell) structure*. *Applied Surface Science*, 2008. **255**(3): p. 781-783.
10. Eastman, J.A., et al., *Anomalously increased effective thermal conductivities of ethylene glycol-based nanofluids containing copper nanoparticles*. *Applied physics letters*, 2001. **78**(6): p. 718-720.
11. Xie, H., et al., *Thermal conductivity enhancement of suspensions containing nanosized alumina particles*. *Journal of Applied Physics*, 2002. **91**(7): p. 4568-4572.
12. Santos, A.P. and C.R. Andrade, *Analysis of gas turbine performance with inlet air cooling techniques applied to Brazilian sites*. *Journal of Aerospace Technology and Management*, 2012. **4**(3): p. 341-353.
13. Xu, G., et al., *Performance evaluation of a nanofluid-based direct absorption solar collector with parabolic trough concentrator*. *Nanomaterials*, 2015. **5**(4): p. 2131-2147.
14. Duffie, J.A. and W.A. Beckman, *Solar engineering of thermal processes*. 2013: John Wiley & Sons.
15. Kalogirou, S.A., *Solar thermal collectors and applications*. *Progress in energy and combustion science*, 2004. **30**(3): p. 231-295.
16. Kennedy, C. and H. Price. *Progress in development of high-temperature solar-selective coating*. in *International Solar Energy Conference, Orlando, Florida USA*. 2005.

17. Minardi, J.E. and H.N. Chuang, *Performance of a “black” liquid flat-plate solar collector*. Solar Energy, 1975. **17**(3): p. 179-183.
18. Abdelrahman, M., P. Fumeaux, and P. Suter, *Study of solid-gas-suspensions used for direct absorption of concentrated solar radiation*. Solar Energy, 1979. **22**(1): p. 45-48.
19. Miller, F. and R. Koenigsdorff, *Theoretical analysis of a high-temperature small-particle solar receiver*. Solar Energy Materials, 1991. **24**(1-4): p. 210-221.
20. Tyagi, H., P. Phelan, and R. Prasher, *Predicted efficiency of a low-temperature nanofluid-based direct absorption solar collector*. Journal of solar energy engineering, 2009. **131**(4): p. 041004.
21. Otanicar, T.P., et al., *Nanofluid-based direct absorption solar collector*. Journal of renewable and sustainable energy, 2010. **2**(3): p. 033102.
22. Moradi, A., et al., *Carbon-nanohorn based nanofluids for a direct absorption solar collector for civil application*. Journal of nanoscience and nanotechnology, 2015. **15**(5): p. 3488-3495.
23. Tiwari, A.K., P. Ghosh, and J. Sarkar, *Solar water heating using nanofluids—a comprehensive overview and environmental impact analysis*. Int J Emerg Technol Adv Eng, 2013. **3**(3): p. 221-4.
24. Wong, K.V. and O. De Leon, *Applications of nanofluids: current and future*. Advances in Mechanical Engineering, 2010. **2**: p. 519659.
25. Wang, X., R. Wang, and J. Wu, *Experimental investigation of a new-style double-tube heat exchanger for heating crude oil using solar hot water*. Applied thermal engineering, 2005. **25**(11): p. 1753-1763.
26. Taylor, R., et al., *Small particles, big impacts: a review of the diverse applications of nanofluids*. Journal of Applied Physics, 2013. **113**(1): p. 1.
27. Mahian, O., et al., *A review of the applications of nanofluids in solar energy*. International Journal of Heat and Mass Transfer, 2013. **57**(2): p. 582-594.
28. Khullar, V., et al., *Solar energy harvesting using nanofluids-based concentrating solar collector*. Journal of Nanotechnology in Engineering and Medicine, 2012. **3**(3): p. 031003.
29. Gan, Y. and L. Qiao, *Radiation-enhanced evaporation of ethanol fuel containing suspended metal nanoparticles*. International Journal of Heat and Mass Transfer, 2012. **55**(21): p. 5777-5782.
30. Elmir, M., R. Mehdaoui, and A. Mojtabi, *Numerical simulation of cooling a solar cell by forced convection in the presence of a nanofluid*. Energy Procedia, 2012. **18**: p. 594-603.
31. Luo, Z., et al., *Performance improvement of a nanofluid solar collector based on direct absorption collection (DAC) concepts*. International Journal of Heat and Mass Transfer, 2014. **75**: p. 262-271.
32. Rahman, M., et al., *Augmentation of natural convection heat transfer in triangular shape solar collector by utilizing water based nanofluids having a corrugated bottom wall*. International Communications in Heat and Mass Transfer, 2014. **50**: p. 117-127.
33. Faizal, M., et al., *Energy, economic and environmental analysis of metal oxides nanofluid for flat-plate solar collector*. Energy Conversion and Management, 2013. **76**: p. 162-168.

34. Parvin, S., R. Nasrin, and M. Alim, *Heat transfer and entropy generation through nanofluid filled direct absorption solar collector*. International Journal of Heat and Mass Transfer, 2014. **71**: p. 386-395.
35. Ladjevardi, S., et al., *Applicability of graphite nanofluids in direct solar energy absorption*. Solar Energy, 2013. **94**: p. 327-334.
36. Bandarra Filho, E.P., et al., *Experimental investigation of a silver nanoparticle-based direct absorption solar thermal system*. Energy Conversion and Management, 2014. **84**: p. 261-267.
37. Karami, M., et al., *A new application of carbon nanotubes nanofluid as working fluid of low-temperature direct absorption solar collector*. Solar Energy Materials and Solar Cells, 2014. **121**: p. 114-118.
38. Said, Z., et al., *Analyses of exergy efficiency and pumping power for a conventional flat plate solar collector using SWCNTs based nanofluid*. Energy and Buildings, 2014. **78**: p. 1-9.
39. Tang, B., et al., *A full-band sunlight-driven carbon nanotube/PEG/SiO₂ composites for solar energy storage*. Solar Energy Materials and Solar Cells, 2014. **123**: p. 7-12.
40. Saidur, R., et al., *Evaluation of the effect of nanofluid-based absorbers on direct solar collector*. International Journal of Heat and Mass Transfer, 2012. **55**(21): p. 5899-5907.
41. Nasrin, R., S. Parvin, and M. Alim, *Effect of Prandtl number on free convection in a solar collector filled with nanofluid*. Procedia Engineering, 2013. **56**: p. 54-62.
42. Hordy, N., et al., *High temperature and long-term stability of carbon nanotube nanofluids for direct absorption solar thermal collectors*. Solar Energy, 2014. **105**: p. 82-90.
43. Liu, Z.-H., et al., *Thermal performance of an open thermosyphon using nanofluid for evacuated tubular high temperature air solar collector*. Energy Conversion and Management, 2013. **73**: p. 135-143.
44. Nagarajan, P., et al., *Nanofluids for solar collector applications: a review*. Energy Procedia, 2014. **61**: p. 2416-2434.
45. Chaji, H., et al., *Experimental study on thermal efficiency of flat plate solar collector using TiO₂/water nanofluid*. Modern Applied Science, 2013. **7**(10): p. 60.
46. Yousefi, T., et al., *An experimental investigation on the effect of pH variation of MWCNT-H₂O nanofluid on the efficiency of a flat-plate solar collector*. Solar Energy, 2012. **86**(2): p. 771-779.
47. Kabeel, A. and E.M. El-Said, *Applicability of flashing desalination technique for small scale needs using a novel integrated system coupled with nanofluid-based solar collector*. Desalination, 2014. **333**(1): p. 10-22.
48. Haider, A.J., L.Z.N. Jameel, and S.Y. Taha, *Synthesis of TiO₂ Nanoparticles by Using Sol-Gel Method and Its Applications as Antibacterial Agents*. 2014.
49. Wu, D., et al., *Critical issues in nanofluids preparation, characterization and thermal conductivity*. Current Nanoscience, 2009. **5**(1): p. 103-112.
50. Khanafer, K., K. Vafai, and M. Lightstone, *Buoyancy-driven heat transfer enhancement in a two-dimensional enclosure utilizing nanofluids*. International journal of heat and mass transfer, 2003. **46**(19): p. 3639-3653.

51. Chen, W., et al. *Numerical Simulation on the Performance of Nanofluid-Based Direct Absorption Solar Collector With Parabolic Trough Concentrator*. in *ASME 2016 5th International Conference on Micro/Nanoscale Heat and Mass Transfer*. 2016. American Society of Mechanical Engineers.
52. Mercatelli, L., et al., *Absorption and scattering properties of carbon nanohorn-based nanofluids for direct sunlight absorbers*. *Nanoscale research letters*, 2011. **6**(1): p. 282.
53. Fluent, A., *Ansys fluent theory guide*. ANSYS Inc., USA, 2011. **15317**: p. 724-746.
54. Duffie, J.A. and W.A. Beckman, *Solar engineering of thermal processes*. 1980.
55. Daniel, P., Y. Joshi, and A.K. Das, *Numerical investigation of parabolic trough receiver performance with outer vacuum shell*. *Solar Energy*, 2011. **85**(9): p. 1910-1914.

